

Characterizing mesoscale eddies of eastern upwelling origins in the Atlantic Ocean and their role in offshore transport

Artemis Ioannou^{1*}, Sabrina Speich^{2, 1}, Remi Laxenaire¹

¹UMR8539 Laboratoire de météorologie dynamique (LMD), France, ²Ecole Normale Supérieure, PSL Research University, France

Submitted to Journal:
Frontiers in Marine Science

Specialty Section:
Physical Oceanography

Article type:
Original Research Article

Manuscript ID:
835260

Received on:
14 Dec 2021

Revised on:
12 Apr 2022

Journal website link:
www.frontiersin.org

Conflict of interest statement

The authors declare that the research was conducted in the absence of any commercial or financial relationships that could be construed as a potential conflict of interest

Author contribution statement

AI and SS designed the study and contributed to the writing. AI performed the data analysis while RL provided TOEddies dataset and automatic eddy detection for the study area. All authors contributed to the article and approved the submitted version.

Keywords

mesoscale eddies, Eastern Boundary Upwelling Systems, oceanic connectivity, cross-basin exchanges, subduction, BCUS cyclones

Abstract

Word count: 224

Motivated by the recurrent formation of eddies in the eastern upwelling areas, we examine cross-basin connectivity that is promoted by coherent, long-lived and long-propagating mesoscale eddies in the Atlantic Ocean.

We use the TOEddies detection and tracking algorithm applied on daily satellite observations (AVISO/DUACS) of Absolute Dynamic Topography (ADT), to characterize mesoscale eddy activity and variability in the North and South Atlantic. This method provides a robust eddy network reconstruction, enabling the tracking of eddies formed in the Atlantic eastern upwelling systems together with any merging and splitting events they undergo during their lifetime as long as they remain detectable in the altimetry field. Among the years of observations, we show that mesoscale eddies are long-lived coherent structures that can ensure oceanic connectivity between the eastern and the western boundaries, and this through complex interactions among eddies. Moreover, colocalization of South Atlantic eddies with eastern boundary origins with available Argo floats reveals a mean cross-basin connectivity signal that is achieved by both anticyclonic and cyclonic eddies which is particular evident at depth, along thermocline isopycnal layers of $\sigma_0 = 26-27 \text{ kg m}^{-3}$. We explore two individual cyclonic eddy trajectories from in-situ measurements achieved by different Argo profiling floats that were trapped inside their eddy cores. Our results support the hypothesis that mesoscale eddies sustain and transport water masses while subducting during their westward propagation.

Contribution to the field

This study aims to investigate how mesoscale eddies from the eastern upwelling current systems (EBUS) may assist on oceanic connectivity across basins in the Atlantic Ocean. So far numerous oceanographic campaigns have been dedicated to EBUS eddies. Nevertheless, there are only few studies that follow them among years of observations. Thanks to TOEddies Atlas we are not only able to characterise and track EBUS eddies but also identify complex eddy-eddy interactions they may undergo. A complex eddy network that concerns only upwelled eddies and eddies connected through merging or splitting events allows for an original assessment of their main routes in the Atlantic ocean. Moreover, eddy colocalisation with Argo float measurements, reveals a mean connectivity signal achieved by both eddy types. Surface and subsurface comparison of their mean vertical structure shows that heat and salt anomalies brought by these eddies can extend further deep below the thermocline. Two EBUS cyclones tracked from satellite observations and sampled by in-situ observations allow us to characterise their temporal evolution providing additional evidence of such transport. Our study highlights that eddies could subduct along their westward propagation while retaining large heat and salt anomalies in their cores.

Ethics statements

Studies involving animal subjects

Generated Statement: No animal studies are presented in this manuscript.

Studies involving human subjects

Generated Statement: No human studies are presented in this manuscript.

Inclusion of identifiable human data

Generated Statement: No potentially identifiable human images or data is presented in this study.

Data availability statement

Generated Statement: The datasets presented in this study can be found in online repositories. The names of the repository/repositories and accession number(s) can be found in the article/supplementary material.

In review

Characterizing mesoscale eddies of eastern upwelling origins in the Atlantic Ocean and their role in offshore transport

Artemis Ioannou^{1,*}, Sabrina Speich¹ and Remi Laxenaire¹

¹*Laboratoire de Météorologie Dynamique LMD-IPSL, Ecole Normale Supérieure, Paris, 75005, France*

Correspondence*:

Artemis Ioannou
innartemis@gmail.com

2 ABSTRACT

3 Motivated by the recurrent formation of eddies in the eastern upwelling areas, we examine
4 cross-basin connectivity that is promoted by coherent, long-lived and long-propagating mesoscale
5 eddies in the Atlantic Ocean. We use the TOEddies detection and tracking algorithm applied
6 on daily satellite observations (AVISO/DUACS) of Absolute Dynamic Topography (ADT), to
7 characterize mesoscale eddy activity and variability in the North and South Atlantic. This method
8 provides a robust eddy network reconstruction, enabling the tracking of eddies formed in the
9 Atlantic eastern upwelling systems together with any merging and splitting events they undergo
10 during their lifetime as long as they remain detectable in the altimetry field. Among the years
11 of observations, we show that mesoscale eddies are long-lived coherent structures that can
12 ensure oceanic connectivity between the eastern and the western boundaries, and this through
13 complex interactions among eddies. Moreover, colocalization of South Atlantic eddies with eastern
14 boundary origins with available Argo floats reveals a mean cross-basin connectivity signal that
15 is achieved by both anticyclonic and cyclonic eddies which is particular evident at depth, along
16 thermocline isopycnal layers of $\gamma^n = 26 - 27 \text{ kg m}^{-3}$. We explore two individual cyclonic eddy
17 trajectories from in-situ measurements achieved by different Argo profiling floats that were trapped
18 inside their eddy cores. Our results support the hypothesis that mesoscale eddies sustain and
19 transport water masses while subducting during their westward propagation.

20 **Keywords:** mesoscale eddies, eastern boundary upwelling systems, oceanic connectivity, cross-basin exchanges, subduction, BCUS
21 cyclones

1 INTRODUCTION

22 Eastern boundary upwelling systems (EBUS) are dynamically complex circulation systems characterized
23 by enhanced mesoscale activity (McGillicuddy et al., 2007; Correa-Ramirez et al., 2007; Stramma et al.,
24 2013; Amos et al., 2019). In the Atlantic Ocean, the Canary Current Upwelling system (CCUS) and the
25 Benguela Current Upwelling system (BCUS) are among the major EBUS of the world ocean. These areas
26 support highly productive marine ecosystems and sustain significant fisheries (Hutchings et al., 2009;
27 Harvey et al., 2020). Their particular dynamics, the combined effect of the strong Ekman transport of the

28 surface waters and the upwelled waters along the coast, give rise to various flow instabilities among which
29 the formation of mesoscale eddies (Chaigneau et al., 2009; Chelton et al., 2011; Pegliasco et al., 2015).

30 Eddies in the CCUS and BCUS are expected a priori to be generated by instabilities of the upwelling
31 current fronts (Marchesiello et al., 2003; Marchesiello and Estrade, 2007; Moscoso et al., 2021). Wang
32 et al. (2015, 2021) showed a strong correlation between the frontal activity (estimated from Sea Surface
33 Temperature fields) and the variability of alongshore winds. Nevertheless, both upwelling systems have
34 their own specificities and it is difficult to separate the physical mechanisms that are involved in eddy
35 generation. For instance, the presence of islands near the CCUS upwelling shelf (Canary islands in the
36 north and the Cape Verde in the south), contributes to eddy generation through island-induced mechanisms
37 (Sangrà et al., 2005; Caldeira et al., 2014; Stegner, 2014; Ioannou et al., 2020a,b). Downstream of the
38 Gran Canaria, is observed the shedding of both, cyclonic and anticyclonic eddies (Arístegui et al., 1994,
39 1997; Basterretxea et al., 2002; Barton et al., 2004; Arístegui and Montero, 2005; Sangrà et al., 2005,
40 2007). On the other hand, high eddy occurrences are found near the African coast (Schütte et al., 2016a)
41 where various instabilities and coastal processes are involved in eddy generation (Dilmahamod et al., 2021).
42 Continuous interactions between island-induced eddies and eddies or filaments from the upwelling have
43 been reported to entrain nutrient rich waters further offshore (Arístegui et al., 1994, 1997; Basterretxea
44 et al., 2002; Arístegui and Montero, 2005; Sangrà et al., 2005, 2007). Based on 14 years of satellite
45 observations (1992-2006), Sangrà et al. (2009) noted long-lived eddies from the upwelling to propagate
46 westward. Distinct eddy corridors were documented along which organic matter could be exported into the
47 oligotrophic subtropical gyre in the North Atlantic.

48 In the south Atlantic, the BCUS upwelling regime, especially its southern part, is intrinsically bounded
49 to the Agulhas leakage (Blanke et al., 2009; Veitch and Penven, 2017; Doglioli et al., 2007) that also
50 shapes, together with the regional circulation, the local dynamics which is particularly energetic and
51 dynamically complex. The intrusion of warm and salty Indian water via the spawning of Agulhas Rings
52 from the Agulhas Current retroflection (Laxenaire et al., 2020, 2019, 2018; Guerra et al., 2018; Giulivi and
53 Gordon, 2006; Matano and Beier, 2003; Arhan et al., 1999) along with the BCUS dynamics as well as
54 the complex bathymetry in the Cape Basin (Matano and Beier, 2003) causes strong interactions between
55 cyclonic and anticyclonic eddies (Boebel et al., 2003; Richardson and Garzoli, 2003; Giulivi and Gordon,
56 2006; Souza et al., 2011). Numerous eddies with high cyclonic versus anticyclonic ratio are observed,
57 (3:2 in favor of cyclones (Boebel et al., 2003)), while various exchanges and water mass modification
58 processes take place (Rusciano et al., 2012). Indeed, satellite imagery has revealed the strong influence of
59 the Agulhas Rings presence in the Cape Basin that could also entrain and export cold upwelling waters
60 along its pathway beyond the upwelling shelf (Duncombe Rae et al., 1992). Yet there are only a few studies
61 (Giulivi and Gordon, 2006; Arhan et al., 2011; Souza et al., 2011) that emphasize on the role of cyclonic
62 eddies from the upwelling and their dynamical characteristics. During a recent hydrographic transect along
63 34.5°S, an Agulhas cyclone originated from an instability along the Benguela upwelling system has been
64 observed near the Southern Africa shelf (Manta et al., 2021). Vessel Mounted Acoustic Doppler Profiler
65 (VM-ADCP) measurements revealed intense velocities for the cyclone that reached 80 cm/s at 100 dbar.
66 Strong temperature anomalies extended between 100 - 700 dbar.

67 Till now, with the only exception of the multi-year observations reported in Sangrà et al. (2009), the
68 characterization of eddies with upwelled origins has been occasionally surveyed and there are still open
69 questions on how far such eddies could travel in the Atlantic Ocean. Unlike waves, coherent eddies,
70 characterized by rotational speeds greater than their translating motion (Flierl, 1981; Chelton et al., 2011;
71 Polito and Sato, 2015), can trap water masses in their core for long time periods remaining physically

isolated from outside perturbations while propagating. Few but important observations of Argo floats that were kept trapped inside eddies for significant time periods (Guerra et al., 2018; Nencioli et al., 2018; Laxenaire et al., 2018, 2019; Ioannou et al., 2017) confirms the existence of such long-lived and long-propagating eddies.

Combined hydrographic observations in the CCUS (Basterretxea et al., 2002; Schütte et al., 2016a,b; Karstensen et al., 2017; Brandt et al., 2015) pointed out that upwelled eddies could substantially contribute to the global offshore transport of properties. Given that eddies inhibit lateral exchanges with the outside environment, they might be responsible for the gradual development of anoxic environments within their cores (Schütte et al., 2016b; Karstensen et al., 2017; Brandt et al., 2015). Eddy-resolving numerical models (Gruber et al., 2011; Nagai et al., 2015) have shown that these eddies can act as the main exporters of nutrients and biological components out of the coastal areas. Subduction of upwelling filaments is also suggested as a possible mechanism contributing to the offshore transport of upwelled waters affecting biological productivity by moving phytoplankton and nutrients in or out the euphotic zone. In other upwelling systems, their contribution to the offshore transport of coastal waters rich in nutrients and carbon has also been highlighted (Amos et al., 2019). In the global ocean, increased chlorophyll concentrations have been continuously reported within eddies (McGillicuddy et al., 2007; Cornec et al., 2021a,b; Dufois et al., 2016; Lehahn et al., 2011; Villar et al., 2015). Mesoscale eddies might thus significantly alter the distribution of properties along their propagation. Hence, a further characterization and quantification of eddies shed from upwelling areas is important to understand cross-shore export of properties, dynamical processes shaping local marine ecosystems and marine connectivity.

Satellite altimetry remains a powerful tool for characterizing the ocean mesoscale. Despite its different limitations and uncertainty (Amores et al., 2018; Laxenaire et al., 2018; Stegner et al., 2021), the development of automatic eddy detection algorithms has made the characterization of eddies from satellite altimetry an easier task, allowing to quantify and follow their temporal variability over long time periods. Automatic detection and tracking algorithms can identify eddies via their imprint on sea surface height, locate their center and quantify their main horizontal dynamical parameters such as their size, intensity, surface geostrophic velocity, drifting speed, etc. Recent techniques (Li et al., 2014; Le Vu et al., 2018; Laxenaire et al., 2018; Cui et al., 2019) provide methods to identify merging and splitting events. In this study, we use the TOEddies Global Atlas to detect and follow eddies in the Atlantic Ocean (Laxenaire et al., 2018). The TOEddies Atlas not only provides information on eddy dynamical characteristics together with their merging and splitting events but also reconstructs a complex eddy network, linking eddy trajectories associated with the merging with other eddies or the splitting in two or more eddies. This has been illustrated in Laxenaire et al. (2018) for the particular case of Agulhas Rings. TOEddies is among the few algorithms that has been qualified against an independent dataset, the eddies derived from surface drifter trajectories and dubbed as “loopers” (Lumpkin, 2016). Moreover, in recent years TOEddies has successfully aided the positioning and tracking of eddies in near-real time during several oceanographic cruises (Manta et al., 2021; Stevens et al., 2021). The TOEddies atlas incorporates colocalized available vertical information from Argo floats with the eddy detection (Laxenaire et al., 2018, 2020). Indeed, the combination of satellite altimetry with autonomous measurements has been proven useful for analyzing the vertical properties of eddies (Chaigneau et al., 2011; Pegliasco et al., 2015; de Marez et al., 2019; Laxenaire et al., 2019, 2020)

Pegliasco et al. (2015) investigated the vertical structure of eddies originating from the major EBUS in the global ocean. By comparing surface and subsurface characteristics of long-lived eddies from the four upwelling systems, the authors found a high percentage of anticyclonic and cyclonic eddies to be

116 subsurface-intensified. Surface intensified eddies that experience summer restratification might potentially
117 separate from the surface, becoming subsurface intensified eddies and retaining an homogeneous water
118 layer in their core. Such mode water eddies, as they are called in the scientific literature, were surveyed in
119 the Canary upwelling system (Schütte et al., 2016a,b; Karstensen et al., 2017; Dilmahamod et al., 2021) and
120 in the Cape Basin (Laxenaire et al., 2019, 2020). Karstensen et al. (2017) surveyed an anticyclonic mode
121 water eddy reporting low oxygen in the eddy core that originated from the Mauritanian upwelling region.
122 Barceló-Llull et al. (2017) also discussed a subtropical intrathermocline four months old anticyclonic
123 eddy in the Canary eddy corridor in 2014. In the south Atlantic, Laxenaire et al. (2019, 2020) found that
124 Agulhas rings subside gradually in deeper ocean layers transforming in subsurface intensified eddies along
125 their westward propagation. This is associated with an important decrease in their surface imprint on
126 altimetry maps and other properties such as sea surface temperature and salinity. Even if the surface signal
127 of such eddies attenuate in time, the reconstructed eddy vertical structure showed no significant changes.
128 The intense heat loss that these eddies experience at the Agulhas Current retroflection and during their
129 displacement in the southern Cape Basin area can lead to an important cooling and increased density of the
130 ring upper 400-600 m layers (Arhan et al., 2011). This induces the transition by subsidence from surface to
131 subsurface eddies while drifting westward and encountering the warmer South Atlantic subtropical gyre
132 waters (Laxenaire et al., 2019, 2020). This introduces a new challenge when identifying mesoscale eddies
133 from satellite observations as the altimetric signal can capture as well as surface-intensified eddies and
134 subsurface-intensified ones (Assassi et al., 2016; Dilmahamod et al., 2018; Laxenaire et al., 2020). Also,
135 when the eddy signal disappears from altimetry maps, this is very likely not due to the eddy dissipation but
136 to its increased penetration at depth.

137 In this paper, we examine the contribution of mesoscale eddies with origins in the EBUS to the offshore
138 export, transport and distribution of properties in the Atlantic Ocean. This is achieved by characterizing
139 mesoscale eddy horizontal and vertical extent with the combination of satellite altimetry and Argo floats
140 measurements using the TOEddies Atlas (Laxenaire et al., 2018, 2020). We focus on the two major eastern
141 boundary upwelling systems of the Atlantic Ocean; namely the Benguela Current Upwelling System
142 (BCUS) and the Canary Current Upwelling System (CCUS) that are characterized by enhanced mesoscale
143 activity. We thus explore the oceanic connectivity that is potentially promoted by coherent, long-lived and
144 long-propagating mesoscale eddies across basins.

145 The paper is organized as follows: in section 2 we describe the various datasets that we used, we introduce
146 TOEddies Dynamical Atlas and the available Argo float measurements. Section 3, presents the dynamical
147 characteristics of eddies in the Atlantic Ocean and in the upwelling systems considered in this study. We
148 discuss the mean horizontal and vertical structure of oceanic connectivity that is achieved by mesoscale
149 eddies of eastern upwelling origins. We present two cyclonic eddies that were sampled by a high number of
150 vertical profiles over one year period along their dynamical evolution in the South Atlantic. We summarize
151 our results and conclude in section 4.

2 DATA AND METHODS

152 2.1 TOEddies Global Dataset and Argo Profiles Colocation

153 To characterize mesoscale eddies, we use the TOEddies Global Atlas dataset (Laxenaire et al., 2018) that
154 provides daily eddy detection and eddy tracking from satellite observations of Sea Surface Height (SSH)
155 over a 24 year period from 1993 to 2018. The TOEddies Global Atlas is applied on fields of Absolute

156 Dynamic Topography (ADT) that are projected on a $\frac{1}{4}^\circ$ ($dX \simeq 25$ km) and distributed by AVISO/DUACS
157 all-sat-merged dataset.

158 Firstly, TOEddies Global Atlas identifies eddies as points of extreme ADT. ADT fields are chosen over
159 the Sea Level Anomaly (SLA) even though the latter has been widely used (Chelton et al., 2011; Cui et al.,
160 2019; Tian et al., 2019). Since SLA fields represent a deviation of SSH from a temporal SSH mean, it could
161 lead to misinterpreting the eddy signal (Pegliasco et al., 2020). Closed contours of SSH that exceed an eddy
162 amplitude threshold, delimit the eddy outer boundary. Once the eddy outer boundary is identified, the SSH
163 contour of maximum azimuthal speed V_{max} is also detected. The latter delimits the eddy dynamical core
164 that physically remains uninterrupted by lateral exchanges with the environment. The outer $\langle R_{out} \rangle$ and
165 characteristic radius $\langle R_{max} \rangle$ of an eddy can be then estimated. The mean radii will correspond to the same
166 area that a circular disc would have when enclosed by the characteristic and the outer contour respectively.
167 In this study, we mainly use R_{max} and V_{max} to quantify respectively the size and the intensity of an eddy.

168 To follow eddies in time, TOEddies requires eddy areas to overlap between successive time steps. This
169 overlapping criterion is additionally combined with a cost-function that takes into account dynamical
170 characteristics such as the eddy size, intensity and distance (Laxenaire et al., 2018; Le Vu et al., 2018) in
171 order to reconstruct the eddy trajectories when eddies split or merge. This technique allows to identify
172 unique segments of eddies instead of eddy occurrences. Eddies that interact with each other, either by a
173 merging or a splitting event, are assigned orders of interactions and can be tracked in the AVISO time-series.
174 This way, the TOEddies algorithm reconstructs a complex eddy network and enables it to track eddies of
175 specific origins (Laxenaire et al., 2018). The accurate detection of merging and splitting events is necessary
176 as successive eddy-eddy interactions can alter the main eddy pathways and impact the reconstruction of the
177 eddy trajectories (Du et al., 2014; Li et al., 2014; Le Vu et al., 2018; Cui et al., 2019).

178 Moreover, TOEddies combines the derived daily eddy detection with vertical information of temperature
179 and salinity from autonomous Argo floats measurements during 2000-2018. For this study, we restrain
180 our analysis to the Atlantic Ocean (80°W - 30°E and 60°S - 60°N) and we use around $\sim 25\%$ of the total
181 colocalisation dataset. It corresponds to 276,259 individual Argo profiles of temperature and salinity
182 collected by 3,024 different floats. The spatial distribution of available profiles in the North and South
183 Atlantic is shown in Figure S1. For each profile, temperature and salinity is converted to potential
184 temperature and absolute salinity using TEOS-10 (McDougall and Barker, 2011). Potential density
185 σ_θ and neutral density γ^n profiles were also estimated. To reconstruct the hydrography of the “no-
186 eddy” environment around a given position and a given date, Argo profiles were separated in two groups:
187 Argo floats that were detected inside mesoscale eddies by TOEddies or outside of them (outside the last
188 eddy contour). The latter are considered to sample the environment and are used to construct climatological
189 profiles of T, S and σ in the given area. Thus, the “no-eddy” climatology consists of all profiles located
190 out of eddies at a radial distance $\leq 1^\circ$ around the selected position and during a ± 30 days period from the
191 given date (regardless of the year) over the 17 years.

192 We have further selected only Argo floats that were located inside eddies from the different eddy network
193 reconstructions that are considered in this study (see subsection 3.3). For analyzing mean vertical properties
194 of the eddy networks, we group profiles in $1^\circ \times 1^\circ$ bins. For each bin and at each depth level, we compute
195 the mean characteristics of temperature and salinity as well as their corresponding anomalies with respect to
196 the climatology. Mean properties were also analyzed in different sigma levels by interpolating all properties
197 to constant density layer intervals ($\Delta\sigma_\theta = 0.01 \text{ kg m}^{-3}$).

198 2.2 Sea Surface Temperature and Atmospheric Data

199 We used ERA-Interim data-set to compute the seasonal and interannual variations of the wind forcing
200 and sea surface temperature for the upwelling areas. This reanalysis provides the atmospheric fields at $\frac{1}{4}^{\circ}$
201 degree spatial resolution and temporal resolution of 1 h. Sea surface wind components at 10 m and sea
202 surface temperature were obtained from the ERA-Interim synoptic fields from 1993 to 2018 (Hersbach
203 et al., 2018). Wind stress components and the wind stress curl were calculated with the standard bulk
204 formula ($\tau = \rho_{air} C_D V_{wind} V_{wind}$ (N m $^{-2}$)) with $\rho_{air} = 1.25$ kg m $^{-3}$ and a constant C_d coefficient ($C_d =$
205 $1.6 \cdot 10^{-3}$). We consider four different sub-upwelling systems; separating the CCUS and BCUS in two
206 sub-systems; the North (nCCUS and nBCUS) and the South (sCCUS and sBCUS) as discussed further
207 in section 3.2 (Figure 6). We build the monthly mean estimates of the wind forcing and the sea surface
208 temperature for the different subsystems and compare their temporal variability.

3 CHARACTERIZATION OF MESOSCALE EDDIES IN THE ATLANTIC OCEAN**209 3.1 Mesoscale activity in the Atlantic Ocean**

210 The TOEddies dynamical dataset detects and tracks more than 14,169,103 eddies (with lifetimes of at
211 least 7 days) and 408,202 eddy trajectories in the Atlantic Ocean.

212 To characterize mesoscale eddy activity, we present in Figure 1, separately for cyclones and
213 anticyclones, histograms of eddy lifetimes, characteristic radii and velocities. Histograms of eddy dynamical
214 characteristics are shown separately for the North and South Atlantic. In these diagrams we have filtered
215 out mesoscale eddies with radius smaller than ≤ 18 km, in order to avoid small-scale features that are
216 not accurately captured by altimetry. We find almost an equal percentage of cyclonic and anticyclonic
217 eddies with lifetimes exceeding 16 weeks even if cyclones are slightly higher in number over anticyclones
218 (cyclonic eddies represent 51.7% of the total for the North and 53.1% for the South Atlantic). Around
219 57% of the tracked eddies are detected in the North Atlantic. In total, eddies with lifetimes less than 4 and
220 16 weeks represent almost 75%, 95% percentile of the eddy lifetime distribution as provided by satellite
221 altimetry maps (Figure S2 and Figure S9). On average, we detect cyclonic eddies with lifetimes more
222 than 16 weeks to have slight smaller radii (by 3%) than anticyclones in both hemispheres, while their
223 characteristics velocities exceed that of the anticyclones mostly in the North Atlantic by 14%.

224 Figure 2 shows trajectories of mesoscale eddies in the Atlantic ocean as tracked by TOEddies. Eastward
225 versus westward trajectories were identified by estimating their net displacement between their first and
226 last position. Eastward propagating eddies with lifetimes ≥ 16 weeks account for only 17.5% of the total
227 trajectories and they correspond mainly to eddies tracked in the Antarctic Circumpolar Current (ACC) and
228 in the subpolar North Atlantic (north of 40°N) (Figure 1). In line with previous studies (Chelton et al.,
229 2011), the majority of long-lived eddies in the North and South Atlantic are found to propagate westward
230 influenced by the β -effect (Figure 2 westward eddies with lifetimes ≥ 52 weeks are shown). The total
231 number of westward propagating eddies in the North Atlantic remains higher than the ones of the South
232 Atlantic (representing 59% of the total westward trajectories).

233 Eddy trajectories were sorted also based on their estimated lifetimes in Figure 3. The lifetime ratio of
234 cyclones versus anticyclones remains similar only for eddies with lifetimes of less than 52 weeks (Figure 1
235 and Figure S2 B and C). In agreement with previous findings (Chelton et al., 2011; Tian et al., 2019),
236 eddies with longer lifetimes (that exceed ≥ 52 weeks, approximately 1.5 years) are mostly anticyclonic
237 (Figure S2). In the South Atlantic, around 60% of eddy trajectories are indeed anticyclonic while in the

238 North Atlantic, the percentage of eddies of both polarities remains close (51% anticyclonic over 49%
 239 cyclonic). Nevertheless, the TOEddies algorithm detects a higher number of long-lived cyclones originating
 240 in the upwelling systems of both hemispheres.

241 Figure 4 compares the cumulative number of Atlantic mesoscale eddy first (A, B) and last detections (C,
 242 D) as well as eddy-eddy interactions (merging and splitting events) (E, F) computed on a $1^\circ \times 1^\circ$ gridded
 243 map as detected daily during the study period (1993 - 2018). In order to account for all possible eddy-eddy
 244 interactions, we count centroids of eddies that were tracked for at least 4 weeks. Hot spots of eddy activity
 245 are characterized by high density of eddy generations exceeding $N > 30$ eddies per degree square. We
 246 found a higher number of eddy generation near the eastern boundary of the ocean basin and, in particular,
 247 within the major eastern upwelling boundary systems (Canary in the North and the Benguela in the South
 248 Atlantic) as well as within the western boundary currents (Brazil Current in the South Atlantic and the Gulf
 249 Stream in the North Atlantic).

250 Several areas where eddies frequently generate are also areas where eddies disappear from the altimetry
 251 maps. Nevertheless, on average the difference between generation and termination points (not shown here)
 252 highlights that the Atlantic EBUS are mostly areas of eddy generation. We note that high spatial distribution
 253 of merging and splitting events also occurs in similar places, a fact that emphasizes the importance of
 254 accounting for eddy-eddy interactions to provide a complete dynamical description of the evolution of the
 255 detected eddies. Merging and splitting events in the North Atlantic involve 53% cyclonic eddies while in
 256 the South Atlantic a similar percentage of 54% is associated with interactions between anticyclonic eddies.

257 Areas of strong mesoscale activity are usually identified by estimating their eddy kinetic energy (EKE).
 258 Similarly with Chelton et al. (2011), we compute the total kinetic energy (KE) from the geostrophic velocity
 259 fields as derived from the daily ADT maps. This is computed by subtracting the temporal mean of the
 260 velocity geostrophic components over the study period

$$KE = \frac{1}{N} \sum_{i=1}^N (u(x, y, t) - \bar{u}(x, y))^2 + (v(x, y, t) - \bar{v}(x, y))^2 \quad (1)$$

261 where $\bar{u} = \frac{1}{N} \sum_{i=1}^N u(x, y, t)$ and $\bar{v} = \frac{1}{N} \sum_{i=1}^N v(x, y, t)$. Based on TOEddies daily eddy detection, we can further
 262 distinguish the percentage of EKE attributed only to anticyclonic and cyclonic eddies respectively and thus
 263 recover areas of eddy kinetic energy associated only to mesoscale eddy activity. This is achieved with a
 264 delta function $\delta(x, y, t)$ that is set to zero when the KE lies outside the eddy last contour and 1 when inside

$$EKE = \frac{1}{N} \sum_{i=1}^N ((u(x, y, t) - \bar{u}(x, y))^2 + (v(x, y, t) - \bar{v}(x, y))^2) \delta(x, y, t) \quad (2)$$

265 We plot in Figure 5, the ratio of eddy kinetic energy versus total kinetic energy separately for cyclonic and
 266 anticyclonic eddies. The eastern upwelling areas are among the most energetic areas in the Atlantic Ocean.
 267 In the CCUS upwelling areas, the signature of both cyclonic and anticyclonic eddies contribute to this
 268 eddy kinetic energy. In the BCUS strong signal of KE is associated mostly with cyclonic eddies near the
 269 upwelling areas, while the intense Agulhas eddy contribution on KE is visible in the right panel of Figure 5.

270 3.2 Dynamical Characteristics of EBUS Trajectories

271 The mean statistical properties of all the eddies detected by TOEddies in the Atlantic ocean shows that
272 the EBUS are areas of increased eddy density due to frequent eddy generations, interactions as well as
273 high EKE. Among them, several long-lived and long-propagating eddies were found to originate from the
274 EBUS.

275 To investigate their role in more details, we firstly define the eddies originating from the upwelling
276 systems. These are defined as eddies that are initially detected within the BCUS and CCUS regions and
277 then propagate into the Atlantic ocean. To represent the upwelling fronts and broadly capture eddies that are
278 generated from instabilities of the shelf, we have chosen the 4000 m isobath. According to previous studies
279 (Cury and Shannon, 2004; Desbiolles et al., 2014; Ndoye et al., 2014), we have additionally separated the
280 BCUS upwelling system in two subsystems; the north and south upwelling cells (nBCUS and sBCUS) at
281 approximately 26.5°S near Lüderitz. This south and north division has been reported to be distinct in terms
282 of climatological wind conditions, regional frontal dynamics (Wang et al., 2015, 2021) but also in terms
283 of biological clustering (Kirkman et al., 2016; Blamey et al., 2015). A similar north and south division is
284 made for the CCUS at around 20°N near Cape Blanc (nCCUS and sCCUS)(Barton et al., 1998; Pelegrí and
285 Benazzouz, 2015; Benazzouz et al., 2014). The different upwelling subregions are illustrated in Figure 6
286 with the different colors (blue for the north and green for the south).

287 In Figure 6 A,B and E,F we display eddy trajectories that originate from the different subsystems and
288 that could be tracked from satellite altimetry maps for more than 16 weeks during the 1993-2018 period.
289 Based on all eddy trajectories, we find both cyclonic and anticyclonic eddies to populate the upwelling
290 subregions. In total numbers, TOEddies tracks more eddies originating from the CCUS subsystems than
291 from the BCUS while the highest number of individual eddy trajectories is found for the nCCUS. The
292 number of tracked cyclones is always found higher than that of the anticyclones while the nCCUS is the
293 only subsystem that is populated by an equal mixture of eddy types (50%/49% cyclones/anticyclones). The
294 asymmetry between cyclonic and anticyclonic eddies is found the strongest for the sBCUS where 83% of
295 the eddies are cyclonic. Slightly lower percentage (67%) is found for the sCCUS, while cyclonic eddies
296 originating for the nBCUS are almost double in numbers over the anticyclonic. This is in line with previous
297 observations (Boebel et al., 2003).

298 Moreover, eddy generation can vary considerably from year to year (Figure 6 C and G). On average, in
299 the sCCUS, the rate of cyclonic eddy generation is close to 8 ± 1.8 eddies per year (lifetimes ≥ 16 weeks in
300 Figure S4). Stronger interannual variations with average rate of 7.7 ± 2.6 cyclones /year are found for the
301 sBCUS. In the nBCUS, this rate is estimated close to 5.3 ± 1.7 cyclones /year. Anticyclonic and cyclonic
302 generation in the nCCUS are similar close to 8 ± 2 eddies /year. Conversely, anticyclonic generation rates
303 remain always below 4.2 ± 1.8 /year for the sCCUS, nBCUS (2.8 ± 1.2 /year) and sBCUS (1.9 ± 1 /year).

304 During specific years, eddies originating from the Atlantic EBUS are tracked for longer periods of time
305 while propagating westward. After generation, cyclones from the sCCUS and nCCUS are mainly translating
306 westward and north-westward, while anticyclones follow very different trajectories and tend to propagate
307 mainly southwestward. Cyclones that are generated in the nBCUS and sBCUS are mainly translating
308 westward and south-westward, towards the southern branch of the South Equatorial Current (Luko
309 et al., 2021; Majumder et al., 2019). Thus, equatorward/poleward deflections for anticyclones/cyclones
310 respectively are also confirmed here in agreement with previous findings (Morrow, 2004; Chaigneau et al.,
311 2009; Chelton et al., 2011; Schütte et al., 2016a). Among them several mesoscale eddies stand out with
312 lifetimes that exceed 2 years and propagation distances that exceed 2000 km (Figure S5).

If we assume that eddy generation in the BCUS and CCUS is mainly driven by instabilities of the upwelling thermal front, we would expect their formation to be associated with the upwelling seasonal variations. We explored the seasonal variations of different indices for the four Atlantic EBUS subsystems explored in the present study (see Supplementary material Figure S6 and Figure S7). The mean monthly variations of all upwelling indicators of the upwelling show the nCCUS and nBCUS upwelling subregions to exhibit a permanent upwelling regime while sCCUS and sBCUS subregions a marked upwelling seasonal cycle (Benazzouz et al., 2014; Pelegrí and Benazzouz, 2015; Brandt et al., 2015).

Even if mesoscale eddies are expected to form more frequently when the upwelling seasonal variations are the strongest, the eddy generation does not exhibit marked seasonal variations (Figure 6). Moreover, when we do detect a seasonal cycle in eddy generation, it does not always coincide with an intenser upwelling seasonal phase (Figure S6). For instance, in the nCCUS, cyclonic and anticyclonic eddy generation peaks in March just after the maximum SSTa that peaks during winter (November/December). Similarly, in the sCCUS cyclonic eddy generation peaks in August, a period of weak upwelling intensity. On the other hand, in sBCUS the cyclonic eddy generation peaks in May, at the end of the most intense upwelling season, when SSTa is found minimum (Figure S6 D). In the nBCUS, an increased cyclonic eddy generation is observed from February till May (peaks in May for AEs), a fact that could be associated with the minimum SSTa during May. Nevertheless, the maximum number of CEs is observed during August which is out of phase with any upwelling index considered (SSTa or WSCa Figures S6 D and E). Even though we do not find a direct correlation, we suspect that the nonlinear processes involved control the eddy generation in the upwelling regions. Marchesiello et al. (2003) has shown that mesoscale eddy variability in the California current system was linked with the alongshore current instabilities. As shown by Marchesiello and Estrade (2007) stratification and topography alone could substantially affect the available potential energy initially provided by the regional wind forcing. This suggests that more thorough investigations are necessary to understand the connections between regional forcing and eddy generation.

In Figure 7, we compare the mean horizontal characteristics of the eddies from the four upwelling subsystems. Histograms of eddy characteristic radii and velocities are plotted separately for cyclonic and anticyclonic eddies. Eddy lifetimes longer than 16 weeks were considered. In the nBCUS and nCCUS, the characteristic radius of cyclonic eddies are estimated around $\langle R_{max} \rangle = 67.1 \pm 23$ km and $\langle R_{max} \rangle = 59.4 \pm 21$ km, 13% and 5% larger from the equivalent average radius of the anticyclones. We found similar sizes (66.3 ± 23 km) for sCCUS cyclones and anticyclones. Cyclones originating from the sBCUS have a mean size of $\langle R_{max} \rangle = 63.4 \pm 22$ km. These are the most intense eddies among the four upwelling systems with mean characteristic velocities reaching almost $\langle V_{max} \rangle = 30 \pm 19$ cm/s, which is twice as high as sCCUS cyclonic eddies (14 ± 7 cm/s), nCCUS (14 ± 15 cm/s) and nBCUS (12 ± 6 cm/s). We note that the mean horizontal characteristics of eddies from the upwellings are associated with large standard deviations indicating that eddy sizes and intensities could substantially vary among the years of observations.

To investigate the mean vertical structure of eddies from each subsystem, we have further selected from the long-lived trajectories of Figure 6 only the ones that were additionally sampled by at least 1 Argo float at a radial distance smaller or equal of the eddy characteristic radius ($d_{argo} \leq R_{max}$). Figure 8 shows the mean vertical structure of temperature and density anomalies of anticyclonic (AEs) and cyclonic eddies (CEs) from each upwelling sub-system. On average, CEs show larger anomalies than the AEs. Moreover, BCUS cyclones seem to contain colder waters from the environment by -1.76°C in the sBCUS and by -1.22°C in the sBCUS in comparison with cyclones from the CCUS the anomalies of which remain below 1°C (-0.46°C and -0.7°C in the sCCUS and nCCUS). On average, CCUS eddies show shallower vertical extents occupying mostly shallower and less dense layers ($\gamma^n = 25.2 - 27.1 \text{ kg m}^{-3}$) in comparison with

357 eddies from the BCUS that extend further deep and larger density intervals ($\gamma^n = 26.5 - 27.14 \text{ kg m}^{-3}$).
358 CEs in sCCUS are characterized by the shallower vertical extent ($\gamma^n = 25.96 \text{ kg m}^{-3} \sim 70 \text{ m depth}$) in
359 comparison with CEs from the sBCUS for which the maximum anomaly in temperature centers at $\gamma^n =$
360 27.07 kg m^{-3} and at almost 430 m depth. We note that all above properties were derived from Argo floats
361 that sampled eddies of the sub-upwelling regions at different radial distances, but always remaining inside
362 the eddy dynamical core. This selection was made in order to retain a relatively large number of Argo floats
363 for each subregion ($N_{Argo} \geq 20$), increasing confidence in the estimated mean EBUS vertical properties.
364 Nevertheless, when taking into account floats located at closer distances from the eddy center ($d_{argo} \leq$
365 $0.5 R_{max}$), we find that the mean eddy hydrological anomalies intensify by at least 30% (they even grow
366 to 60% for the sBCUS and sCCUS subregions). We note that the distance from the eddy center should
367 be taken into further consideration when investigating its impact on nutrients or chlorophyll distribution
368 (Wang et al., 2018).

369 3.3 Mean Upwelled Eddy Connectivity Signal

370 The main exporters of nutrient-rich waters from the CCUS and BCUS seem to be mostly associated
371 with cyclonic features. Nevertheless, apart being areas of frequent eddy generation these EBUS are also
372 associated with large eddy-eddy interactions that lead to numerous eddy splitting and merging events
373 (Figure 4). Such events alter the main eddy pathways and are supposedly linked with important transfer of
374 waters. Hence, identifying merging and splitting events of both eddy types is essential to understand the
375 eddies evolution.

376 Following Laxenaire et al. (2018), we reconstruct an eddy network made of all trajectories that are
377 related with various filiation to eddies of upwelled origins. By assigning orders on eddy-eddy interactions,
378 the resulting eddy trajectories network assembles all eddies connected via a merging or a splitting and
379 traces them from the upwelling areas further offshore in the Atlantic. Figure 9 shows the eddy network
380 reconstruction for the two key areas the BCUS and the CCUS upwelling systems. Trajectories illustrated
381 with the black color are the reference trajectories that originate from the shelf and are assigned an order
382 zero. The order number increases relatively to the number of interactions that are needed to trace back or
383 forward a reference trajectory.

384 In total, the BCUS and the CCUS eddy networks are composed of 11,764 and 12,969 eddy trajectories
385 respectively (with lifetimes larger than 4 weeks). Overall, eddies from upwelling networks account for only
386 10% of the total number of trajectories tracked in the Atlantic by the TOEddies algorithm. However, if we
387 only consider long-lived eddies from these networks (with lifetimes larger than 52 weeks), this percentage
388 increases to 64%. Mesoscale eddies of order zero (originating from the upwelling areas) are mostly cyclonic,
389 counting for 75% of the zero eddy trajectories for the BCUS and 57% for the CCUS (lifetimes ≥ 16 weeks).
390 Nevertheless, anticyclonic eddies are also involved in the advection of properties when higher orders of
391 interactions are considered. Besides, the role of anticyclonic eddies on the advection and entrainment of
392 upwelled waters if situated near the upwelling coastal areas has been previously highlighted for both the
393 CCUS and the BCUS (Arístegui et al., 1997; Duncombe Rae et al., 1992). When accounting for merging
394 and splitting events, both eddy types ensure connections between the eastern and western boundaries
395 contributing to a mean connectivity signal (Figure 9).

396 The EBUS eddy network reconstruction shows that long-lived and long-propagating eddies along with
397 their frequent interactions might potentially transport waters from the upwelling regions further offshore
398 and in some cases even reach the western Atlantic boundaries (Guerra et al., 2018; Nencioli et al., 2018;
399 Laxenaire et al., 2018, 2019). In order to investigate if these connections concern only the upper-ocean

400 dynamics, we selected all Argo floats from the TOEddies colocalisation Atlas that were identified inside
401 the BCUS and CCUS network trajectories (Figure 9). Together, BCUS and CCUS eddy networks were
402 sampled by 28,554 Argo profiles in various positions inside eddies. Around 21% of the total EBUS network
403 trajectories were sampled by at least 1 Argo float. From these 64% sampled anticyclones and 36% cyclones.

404 In order to estimate the mean connectivity signal that these mesoscale eddies bring in comparison with
405 the adjacent environment, in Figure 10 we plot mean anomalies of potential temperature estimated from the
406 CCUS and BCUS eddy networks in the upper layers ($\langle \gamma^n \rangle = 25 - 26 \text{ kg m}^{-3}$) and thermocline isopycnal
407 layers ($\langle \gamma^n \rangle = 26 - 27 \text{ kg m}^{-3}$). Anomalies were computed by subtracting the non-eddy climatology in
408 each isopycnal surface. Positive and negative anomalies of temperature correspond to anticyclonic and
409 cyclonic eddies respectively. These properties concern only Argo floats trapped inside eddy trajectories
410 with origins from the eastern upwelling system (we limited the estimate to up to order 5 trajectories in
411 Figure 9). The subsurface extent of eddy properties is visible well below the surface, reaching intermediate
412 depths.

413 On average, for the CCUS network, anticyclones are associated with mean temperature/salinity anomalies
414 of about $0.45 \pm 0.91 \text{ }^{\circ}\text{C} / 0.02 \pm 0.14 \text{ g/kg}$ in the upper layers and $0.26 \pm 0.47 \text{ }^{\circ}\text{C} / 0.04 \pm 0.09 \text{ g/kg}$ for
415 denser layers. For BCUS, these mean temperature/salinity anomalies are stronger for both, the upper layers
416 ($0.93 \pm 1.29 \text{ }^{\circ}\text{C} / 0.1 \pm 0.18 \text{ g/kg}$) and for denser layers ($0.95 \pm 0.94 \text{ }^{\circ}\text{C} / 0.12 \pm 0.12 \text{ g/kg}$). For CCUS
417 cyclonic eddies, the mean temperature/salinity anomalies were estimated $-0.4 \pm 1 \text{ }^{\circ}\text{C} / -0.004 \pm 0.12 \text{ g/kg}$
418 for the upper layers and slightly weaker at greater depth ($-0.39 \pm 0.6 \text{ }^{\circ}\text{C} / -0.04 \pm 0.1 \text{ g/kg}$). For BCUS
419 anomalies for the cyclones were found even positive in the upper isopycnal layers $0.08 \pm 1 \text{ }^{\circ}\text{C} / -0.04 \pm$
420 0.15 g/kg but reached $-0.67 \pm 0.9 \text{ }^{\circ}\text{C} / -0.08 \pm 0.11 \text{ g/kg}$ for deeper layers.

421 The mean properties from the eddy networks demonstrated the additional contribution and spreading of
422 heat and salt by mesoscale eddies in comparison with the environment. The comparison between upper and
423 deeper isopycnal layer anomalies indicated that cross-basin connectivity achieved by mesoscale eddies
424 does not only concern the upper layers but seems to extend down to the main thermocline. For BCUS
425 cyclones the maximum of intense anomalies was found to be even stronger for the denser layers here
426 considered ($\langle \gamma^n \rangle = 26 - 27 \text{ kg m}^{-3}$) rather than in the upper layers.

427 3.4 Individual Eddy Trajectories

428 In the previous section, by combining available hydrographic properties from Argo floats with the
429 eddy trajectory networks built for the CCUS and BCUS, we estimated the mean temperature and salinity
430 anomaly within isopycnal layers related with mesoscale eddies of EBUS origins in the Atlantic. These
431 mean anomalies of properties provided by eddies are not restrained in the surface layers but can extend
432 through the thermocline. In this section, in order to evaluate further the vertical eddy properties and how
433 they evolve in time we searched among the years of observations for individual eddy trajectories that were
434 sufficiently sampled by Argo floats.

435 From the total eddy trajectories networks, we select specific examples of cyclonic and anticyclonic
436 trajectories that were sampled by more than 30 Argos over periods of more than one year, allowing us to
437 gather information on their internal structure along their en-route propagation. Among them we have firstly
438 recovered several Agulhas Rings that have been previously described in Laxenaire et al. (2019, 2020) and
439 thus omit their discussion in this paper. We have further isolated two specific cases of cyclonic eddies in
440 the years 2012 and 2015 that were sampled by a total of 41 and 44 Argo profiles, the dynamical evolution
441 of which we describe in the following section. To our knowledge these are among the few occurrences

442 where Argo floats remained trapped inside coherent cyclones for significant long time periods, providing
443 us information on their vertical structure and evolution.

444 3.4.1 BCUS Cyclones: Eddy Signature on Subduction

445 Figure 11 A shows the trajectories of two cyclonic eddies, C0 and C1, one originating from the nBCUS
446 and one from the sBCUS and sampled by more than 30 profiles (magenta points) during their lifespan.
447 These two cyclones were formed in late fall, in March 2012 (C1) and April 2015 (C0) respectively. They
448 moved mainly west-southwestward and were tracked for more than 1 year with TOEddies. The movies of
449 the dynamical evolution of the two cyclones (see supporting information) shows their daily tracking by
450 TOEddies in the sea surface height fields along with their sampling rate from the Argo floats.

451 Several snapshots along the temporal evolution of the surface signature of these eddies are presented in
452 Figure 12. Cyclone C0 was initially detected on 5th January 2015 in the nBCUS upwelling frontal zone
453 and was tracked with TOEddies till the 1st April 2016, for almost 65 weeks (approximately 1.5 years). The
454 eddy drifted westward covering a distance of 1.793 km while an Argo float (WMO 1901310) sampled
455 C0 at various radial distances from the eddy center providing in total 44 T, S profiles. According to the
456 TOEddies network reconstruction, this cyclone merged on 25 Feb 2015 with a short-lived cyclone (less
457 than one month old) initially detected on 18 January 2015 (Figure 12 A). It seems that also this eddy
458 detached from the nBCUS slightly south of C0 (11.39° E, 26.55° S) and it was sampled by the same Argo
459 float that later remained trapped in C0 for almost 8 months. During the eddy generation, when the eddy
460 scales remain relatively small and in close distance from the shore, we cannot guarantee that satellite
461 altimetry resolution remains accurate to resolve such rapid interactions between eddies. Nevertheless, this
462 detachment was identified as a merging event by TOEddies. The Argo T/S profiles before and after the
463 merging event showed that the eddy water masses were not significantly impacted. During the months that
464 followed, the eddy propagated westward reaching and crossing the Walvis Ridge during austral winter
465 (June, July August) of 2015 (Figure 12 C and D).

466 Cyclone C1 was initially detected in sBCUS on 27 February 2012, north-west of Cape Town. This
467 cyclone was tracked with TOEddies for almost 71 weeks (16 months). From March 2012 several different
468 Argo floats sampled the eddy till the 12th July 2013 when the eddy was lastly detected, providing 41
469 vertical profiles. From August 2012, the cyclone drifted westward while it started to interact and propagate
470 along with an Agulhas Ring that was in the vicinity (Figure 12 G-H). Such cyclone-anticyclone interactions
471 in the Cape Basin have been previously documented from observations (Boebel et al., 2003; Souza et al.,
472 2011) and numerical simulations (Doglioli et al., 2007).

473 Figure 11 B and C depicts the daily evolution of the geostrophic dynamical characteristics of the radius
474 and azimuthal velocity of the two eddies under investigation. The time series for the cyclones C1 and C0
475 shows distinct dynamical periods for the eddies. During generation, when the eddies move away from the
476 continental slope, variations in their velocity and radius were observed. After generation both cyclones
477 increased in radius and velocity. The latter reached a maximum of 40 cm/s and 60 cm/s for cyclone C0 and
478 C1 respectively, 6 months after generation (Figure 11C). We note that the maximum eddy intensities are
479 at least twice as high than the mean CEs intensities shown in section 3.2. Indeed, for cyclone C0, during
480 austral summer the eddy diameter remains constant whereas the eddy tangential speed increases when the
481 eddy crosses the Walvis Ridge. During that period, its translation speed is relatively weak (~ 7 km/day),
482 and its shape remains almost circular with ellipticity below $\varepsilon = 0.3$. Then a decay in the eddy velocities are
483 observed.

In order to investigate the evolution of the vertical structure of the eddies core, we selected only Argo profiles that were located at a radial distance of less than ≤ 55 km from their estimated centers (Figure 13 A and B). This corresponds to a mean ratio between the Argo radial distance and the eddy characteristic radius of about 50% (maximum ratio of about 74%). The temporal evolution of the temperature and density in the core of the two cyclones is shown in Figure 13 C and D along with the estimation of their mixed layer depth (MLD). The latter was determined by computing the depth where the Brunt–Väisälä frequency squared $(N^2 = -\frac{g}{f} \frac{\partial \rho}{\partial z})$ was found minimum. We then estimate the density anomaly induced by the eddies based on the climatological eddy background that contains non eddy signature (Figure 13 E and F). To quantify the vertical extent of the eddy we compute the depth of the maximal density anomaly.

According to Figure 13 during the first 3 months of the formation of cyclone C0, the density anomaly of the eddy seems weak in comparison with the surrounding environment. This makes sense when considering that the eddy did not detach yet from the shelf and the upwelling tongue: during this period the eddy is mainly trapped in the upwelled waters that are not significantly different from the adjacent environment. Once the eddy starts to propagate westward, we do detect a temperature anomaly located between -200 and -700 m of depth which is -2.8°C / -0.3 g/kg colder and fresher in comparison with the environment. The density anomaly of the cyclone C0 is confined between -100 and -700 m of depth with a maximal density anomaly of $\sigma_A = 0.34 \text{ kg m}^{-3}$ that was located at -190 m in May 2015. Two months later, the maximal density anomaly seems to further deepen, reaching $z_{max} = -210$ m on 30 July 2015. In September 2015, the maximal density anomaly reached a depth of $z_{max} = -240$ m while remaining relatively strong $\sigma_A = 0.37 \text{ kg m}^{-3}$ (with -3.4°C / -0.37 g/kg temperature and salinity anomalies). Unfortunately, no other Argo float was detected inside the eddy after November 2015 despite TOEddies was able to track it till the 1st April 2016 (5.5°W , 27.54°S).

Concerning cyclone C1, one month after its formation (on 22 March 2012), the eddy density anomaly was $\sigma_A = 0.52 \text{ kg m}^{-3}$ at -80 m. Five months later, the maximal σ_A remained the same in intensity while deepened, reaching a depth of $z_{max} = -180$ m on 25 Aug 2012, with corresponding temperature and salinity anomalies of -4.4°C / -0.47 g/kg. In November 2012, the maximal density anomaly deepened further reaching $z_{max} = -250$ m probably as a result of air-sea interactions that cooled and mixed the eddy upper layers, deepening the eddy MLD. Indeed, during that period the upper layers seem to be connected to the surface. From November till at least March 2013 (austral summer), in the upper eddy structure, a seasonal thermocline appears, whereas the eddy core seems to penetrate further in depth while gradually separating from the ocean surface. Afterwards, the eddy propagated southwestward (0.57°E , 37.9°S) till the 12th Jul 2013 when it was last detected.

The vertical sampling of the two BCUS cyclones, C0 and C1, show that these eddies account for density anomalies of $\sigma_A = 0.5 \text{ kg m}^{-3}$ and temperature anomalies of 4.4°C in the Cape Basin. Both cyclonic eddies showed a progressive deepening of their vertical structure and a clear separation from the ocean surface, suggesting that these eddies subside and become subsurface intensified eddies as they leave the upwelling area and penetrate into the Cape Basin. This is accompanied by a gradual decay of both eddy surface intensities whereas subsurface anomalies remain relatively unchanged. Nevertheless during this period the subsurface anomalies remain relatively steady in characteristics showing a progressive inclination of their isopycnals towards deeper layers.

Such a behavior has been already observed and described for anticyclonic eddies, in particular for Agulhas Rings and for CCUS specific anticyclones (Schütte et al., 2016a; Karstensen et al., 2017; Barceló-Llull et al., 2017; Guerra et al., 2018; Laxenaire et al., 2019, 2020). (Laxenaire et al., 2019, 2020) showed that

527 the majority of Agulhas Rings become subsurface intensified eddies along their route. However, the results
528 we discuss in the present study, represent the first evidence of such behavior for cyclonic eddies in the
529 South Atlantic.

In review

4 SUMMARY AND CONCLUSIONS

Motivated by the fact that EBUS are areas of high productivity as well as of frequent eddy generation, we examined cross-basin oceanic connectivity that is promoted by coherent, long-lived and long-propagating mesoscale eddies with eastern upwelling origins in the Atlantic Ocean. We characterized the dynamical properties of mesoscale eddies over a 24 year period (1993 to 2018) in the whole Atlantic with the TOEddies Dynamical Dataset that uses daily satellite observations of ADT.

Among all the mesoscale eddies that are detected in the Atlantic Ocean with TOEddies dataset, a small fraction of them will be long-lived (10% with lifetimes more than 52 weeks). In agreement with previous studies (Chaigneau et al., 2009; Chelton et al., 2011), long-lived eddies are found to propagate mainly westward and to be predominantly anticyclonic. However, at least 60% of these westward long-lived eddies are found to either originate or interact with eddies from the eastern boundary upwelling systems. We have then specifically qualified from the whole Atlantic TOEddies dataset the eddies spawn from the four upwelling subsystems (north and south CCUS and BCUS) analyzing their seasonal and interannual variabilities. By using the colocated Argo floats profiles, also provided by the TOEddies Atlantic atlas, we characterized their mean vertical structures retaining only the Argo profiles sampling the eddies dynamical core.

To estimate the eddy contribution on oceanic connectivity, we reconstructed the eddy trajectory network relating eddies of upwelled origins with all those nearby eddies connected to them via merging/ and splitting events. The mean eddy connectivity signal is then derived based on the synthesis of the CCUS and BCUS eddy networks with 17 years of in-situ observations from Argo floats. The comparison between eddies from the four upwelling subsystems showed that a higher number of eddy trajectories is associated mostly with cyclonic rather than anticyclonic eddies. To this, the nCCUS subsystem was found as the only exception characterized by an equal mixture of eddies with different polarity. In total numbers, more eddies are detected to originate from the CCUS compared with the BCUS. On the other hand, our study suggests that sBCUS is mainly characterized by cyclonic eddies (83%), the mean tangential velocity of which is about double the intensity of cyclones spawn from the other subsystems. Our comparisons with the mean upwelling indicators as derived from ERA5 datasets showed that the seasonal variations of the eddy formation do not always coincide with the mean upwelling climatology. Further investigation of possible connections between specific eddy formations and the processes responsible for their variability is required (Marchesiello et al., 2003; Marchesiello and Estrade, 2007; Moscoso et al., 2021).

We do recover the Canary eddy corridor as firstly introduced in Sangrà et al. (2009) for the CCUS, while we track long-lived eddies to propagate even farther than 35°W. Similar eddy westward pathways are found for the BCUS. Poleward/equatorward deflections for cyclonic/anticyclonic eddies are also confirmed in our study. Nevertheless, cyclones originating from the sCCUS and nBCUS are found to propagate mostly westward, also joining the southern branch of the South Equatorial Current (Luko et al., 2021; Majumder et al., 2019). Several of the upwelled origin eddies we investigate, contribute to a mean oceanic connectivity across basins as when they succeed to reach the western boundary current systems. Eddy mean lifetimes could exceed 1 year and propagations distances of 2000 km. Moreover, we have seen that these eddies are not isolated but often merge and split with other structures. When taking into account eddy-eddy interactions, both cyclonic and anticyclonic eddies are found to be both important in transporting water properties across-basins. The mean thermohaline structure as derived from the combination of eddy trajectories with available Argo float measurements displays a mean connectivity signal between eastern and western boundaries that does not concern only surface layers but it can extend further deep. On average the vertical extent of eddies from the CCUS is found shallower (maximum temperature anomalies ranging

573 between 50 - 190 m, $\gamma^n = 25.2 - 27.1 \text{ kg m}^{-3}$) than that from the BCUS that occupy deeper and denser
574 layers (150 - 530 m, $\gamma^n = 26.5 - 27.14 \text{ kg m}^{-3}$). Mean anomalies associated with BCUS cyclonic eddies
575 were found even stronger along the lower thermocline isopycnal layers ($\gamma^n = 26.5 - 27 \text{ kg m}^{-3}$).

576 Finally, we focus on two specific years where two cyclonic eddies that originated from the nBCUS
577 and sBCUS were formed. During these years, Argo profilers were trapped for several months in their
578 cores allowing us to compare the temporal evolution of their hydrological properties. The two cyclonic
579 eddies that were sampled by Argo floats along their en-route propagation provided additional observational
580 evidence of transport of properties by coherent eddies. The temporal evolution of their anomalies revealed
581 a progressive deepening of the eddy core into deeper thermocline layers while being advected further
582 west, suggesting a subduction and a transformation of these eddies from surface intensified to subsurface
583 intensified structures. Cyclone C0 originating from the nBCUS crossed the Walvis Ridge and left the Cape
584 Basin contrary to previous findings (Matano and Beier, 2003). Moreover, the multi-month vertical sampling
585 of this eddy by Argo floats showed that the core of the eddy remained unchanged while crossing the Walvis
586 Ridge. The subduction process has been evidenced for Agulhas Rings (Laxenaire et al., 2019, 2020) but,
587 to our knowledge, this study represents the first description of subduction for cyclonic eddies. Besides,
588 subsurface eddies have already been surveyed in similar EBUS areas, as for example in CCUS (Schütte
589 et al., 2016a,b; Karstensen et al., 2017; Dilmahamod et al., 2021).

590 We note that our study provides information only for a small fraction of eddies whose signature is
591 detectable from altimetry maps. Nevertheless, our results suggest that the Atlantic eastern boundary
592 upwelling systems are important sources of long-lived eddies that might efficiently export heat, salt and
593 other water properties further offshore from the coastal upwelling areas. As documented in this study for
594 two cyclonic eddies spawn from BCUS, or Agulhas Rings (Laxenaire et al., 2019, 2020) or anticyclones in
595 CCUS (Schütte et al., 2016a,b; Karstensen et al., 2017; Dilmahamod et al., 2021), many eddies subduct
596 into the subsurface while drifting westward. Hence, we suggest that most of the eddies that disappear
597 from the altimetry maps do not immediately dissipate but continue to drift into the open ocean masked
598 by the upper-ocean layers stratification. Their potential impact on thermocline ventilation and coastal
599 ecosystems should be addressed in future studies. Indeed, these eddies trap and advect water properties as
600 well as plankton and fish larvae from the nutrient-rich upwelling shelves. Their ability in connecting distant
601 environments should be investigated further.

CONFLICT OF INTEREST STATEMENT

602 The authors declare that the research was conducted in the absence of any commercial or financial
603 relationships that could be construed as a potential conflict of interest.

AUTHOR CONTRIBUTIONS

604 AI and SS designed the study and contributed to the writing. AI performed the data analysis while RL
605 provided TOEddies dataset and automatic eddy detection for the study area. All authors contributed to the
606 article and approved the submitted version.

FUNDING

607 This paper was supported by the TRIATLAS project, which has received funding from the European
608 Union's Horizon 2020 research and innovation programme under grant agreement No 817578.

ACKNOWLEDGMENTS

609 We would like to gratefully acknowledge and thank the two reviewers for their comments that helped us
610 improve the manuscript and Johannes Karstensen from the GEOMAR Helmholtz Centre for Ocean Research
611 in Kiel for his helpful suggestions and bibliographic input. This work was supported by the European
612 Union's Horizon 2020 research and innovation program under grant agreements no. 817578 (TRIATLAS),
613 the TOEddies and BIOSWOT CApeCauldron CNES-TOSCA and the ENS Chaire Chanel research grants.
614 We also acknowledge the mesoscale calculation server CICLAD (<http://ciclad-web.ipsl.jussieu.fr>) dedicated
615 to Institut Pierre Simon Laplace modeling effort for technical and computational support.

DATA AVAILABILITY STATEMENT

616 The data used for this paper are available at the following repository and can be accessed through the
617 following link (10.5281/zenodo.6443096). The gridded satellite altimetry data we used in this work
618 were produced by SSALTO/DUACS and distributed by the Copernicus Marine Environment Monitoring
619 Service (<http://www.marine.copernicus.eu>). The Argo data were collected and made freely available by the
620 International Argo Program and the national programs that contribute to it (<https://coriolis.eu.org>).

FIGURE CAPTIONS

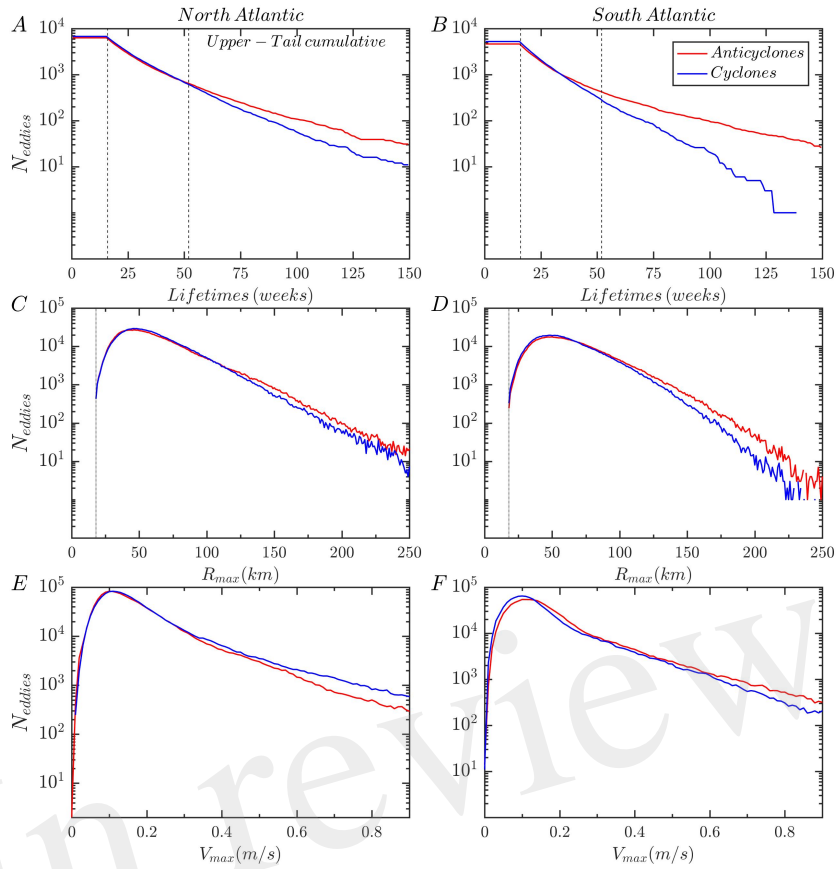


Figure 1. Upper-tail cumulative histograms of the eddy lifetimes (weeks) (panels A and B) and histograms of eddy characteristic radius R_{max} (km) (panels C and D) and velocity V_{max} (m/s) (panels E and F) of anticyclonic (red colors) and cyclonic eddies (blue colors) for the North (left panels) and South (right panels) Atlantic Ocean during 1993-2018 period. We consider only mesoscale eddies having lifetimes ≥ 16 weeks and characteristic radius larger than $R_{max} \geq 18$ km as illustrated with the dashed lines in panels A, B and C and D respectively.

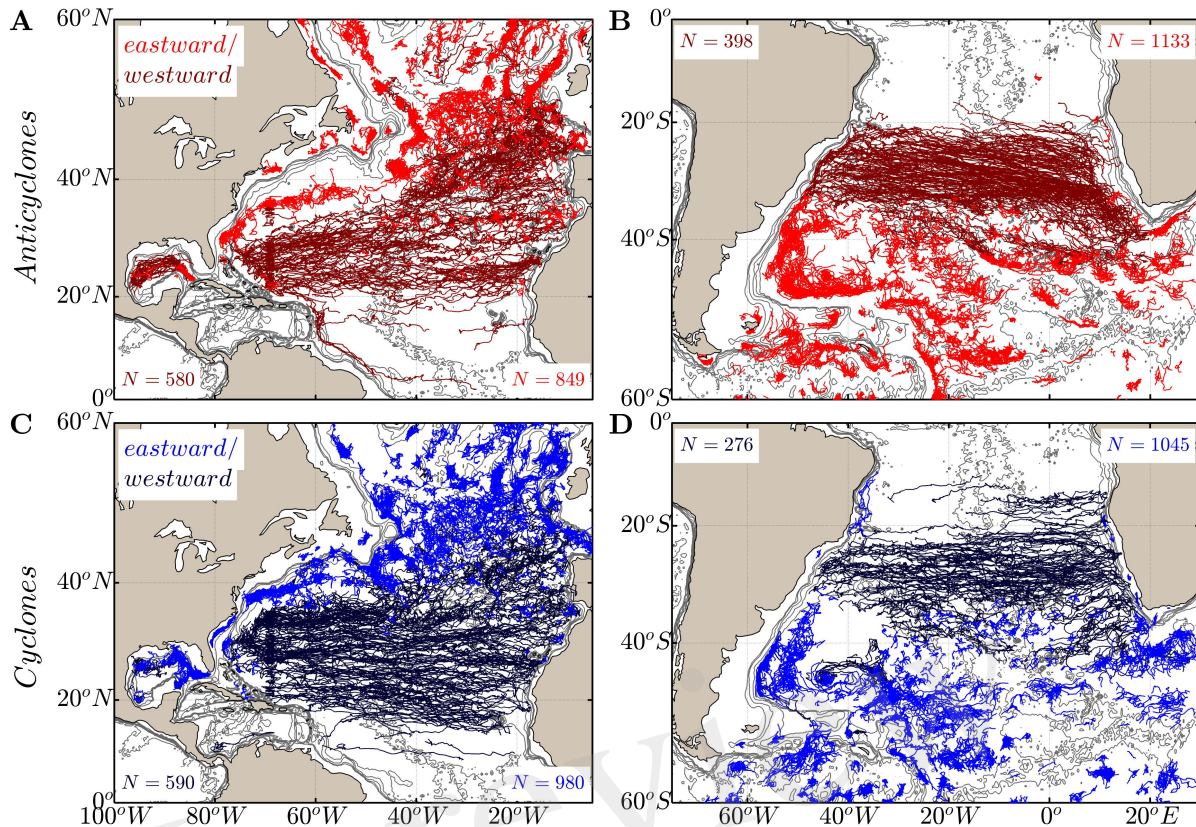


Figure 2. Trajectories of eastward (lighter colors) versus westward (denser colors) propagating eddies with lifetimes longer than ≥ 16 weeks and longer than ≥ 52 weeks respectively. Anticyclonic (panels A, B) and cyclonic (panels C, D) are illustrated with the blue and red colors as detected from TOEddies algorithm over a 24 year period (1993-2018). The bathymetry that is shallower than 4000 m is illustrated with the gray lines.

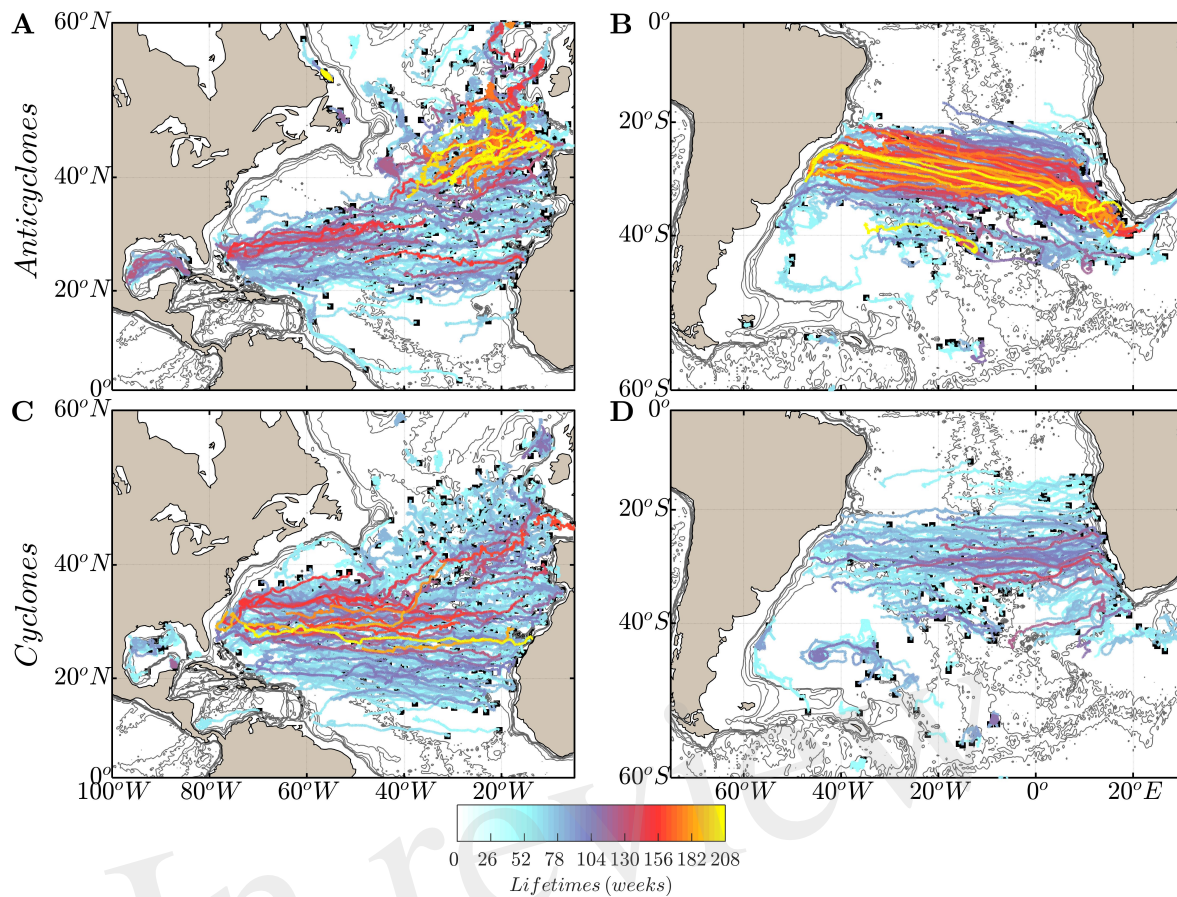


Figure 3. Trajectories of anticyclonic (panels A and B) and cyclonic (panels C and D) eddies as detected from TOEddies algorithm over a 24 year period (1993–2018) having a lifetime longer than ≥ 52 weeks. Each trajectory is colored based on their estimated lifetimes (weeks). The bathymetry that is shallower than 4000 m is illustrated with the gray lines.

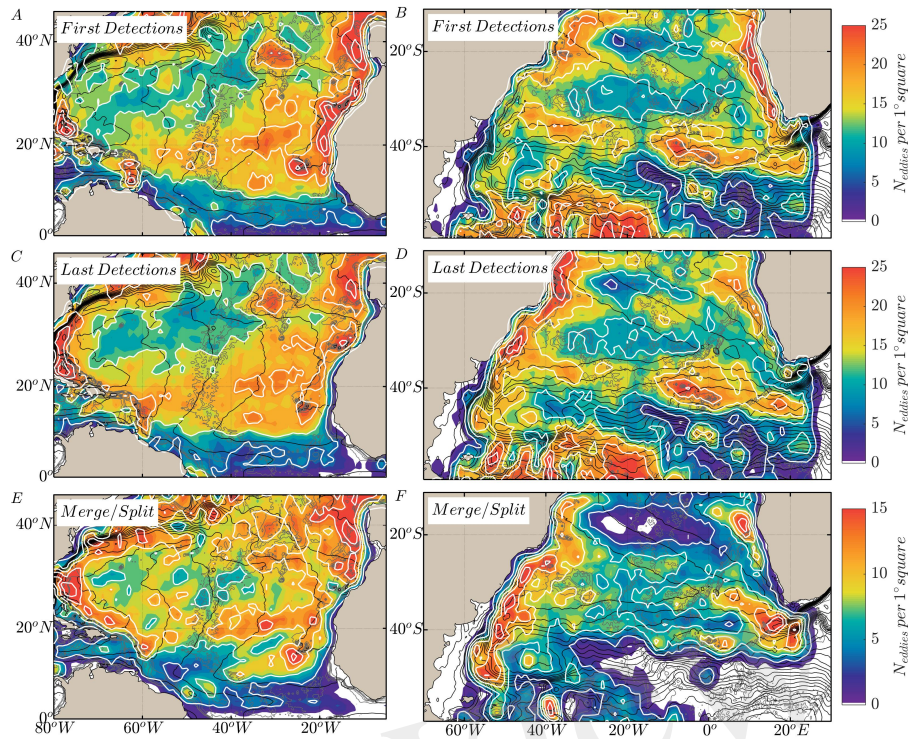


Figure 4. Frequency maps of first (panel A), last (panel B) detection points and merging and splitting points (panel C) of mesoscale eddies with lifetimes longer than ≥ 4 weeks as detected in the South and North Atlantic from the TOEddies global Atlas over the 24 year period (1993-2018) gridded over $1^\circ \times 1^\circ$ bins (smoothed using a $1^\circ \times 1^\circ$ window). The mean dynamic topography MDT (cm) is shown with the black contours and the bathymetry shallower than 4000 m depth with the gray lines.

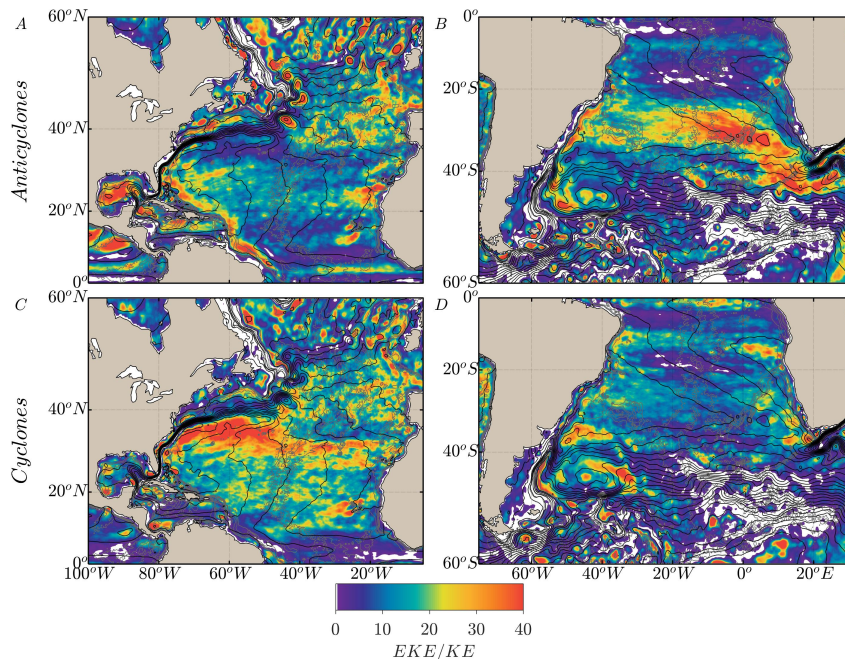


Figure 5. Ratio of mesoscale eddy kinetic energy (EKE) contribution to the total kinetic energy (KE) in the North (left panels) and South Atlantic (right panels) respectively for anticyclonic (panels A and B) and cyclonic (panels C and D) eddies gridded over $1^\circ \times 1^\circ$ bins. The mean dynamic topography MDT (cm) is shown with the black contours and the bathymetry shallower than 4000 m depth with the gray lines.

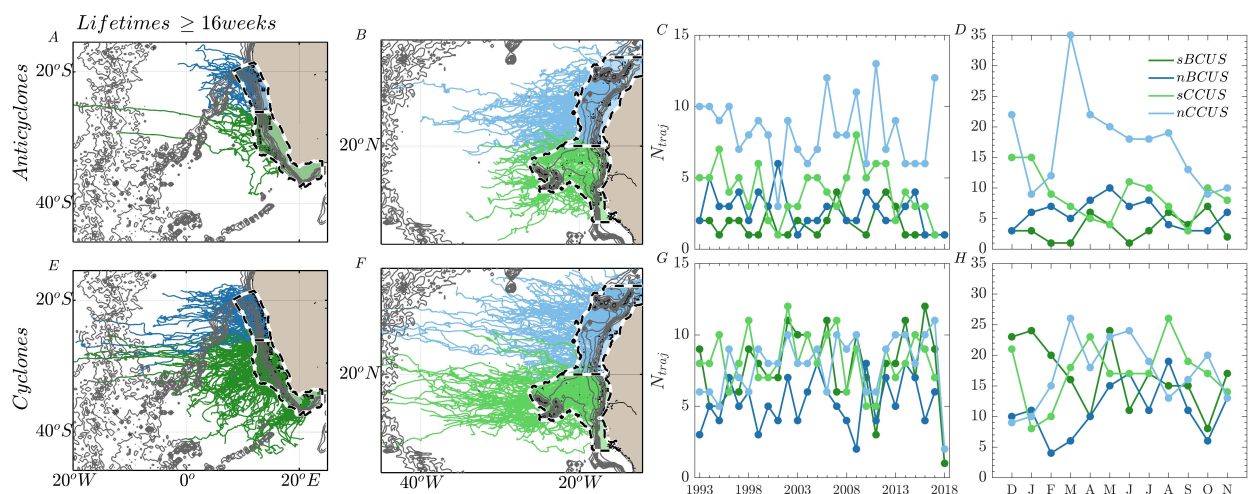


Figure 6. Eddy trajectories originating from the four sub-upwelling systems: nBCUS and sBCUS (panels A and E) and sCCUS and nCCUS (panels B and F) as obtained from TOEddies Global Atlas with lifetimes more than ≥ 16 weeks. The mean annual and monthly number of eddies is illustrated in panels C, G and D, H respectively for anticyclonic and cyclonic trajectories. The north and south upwelling regions of the BCUS and CCUS are illustrated with the blue and green patch areas respectively.

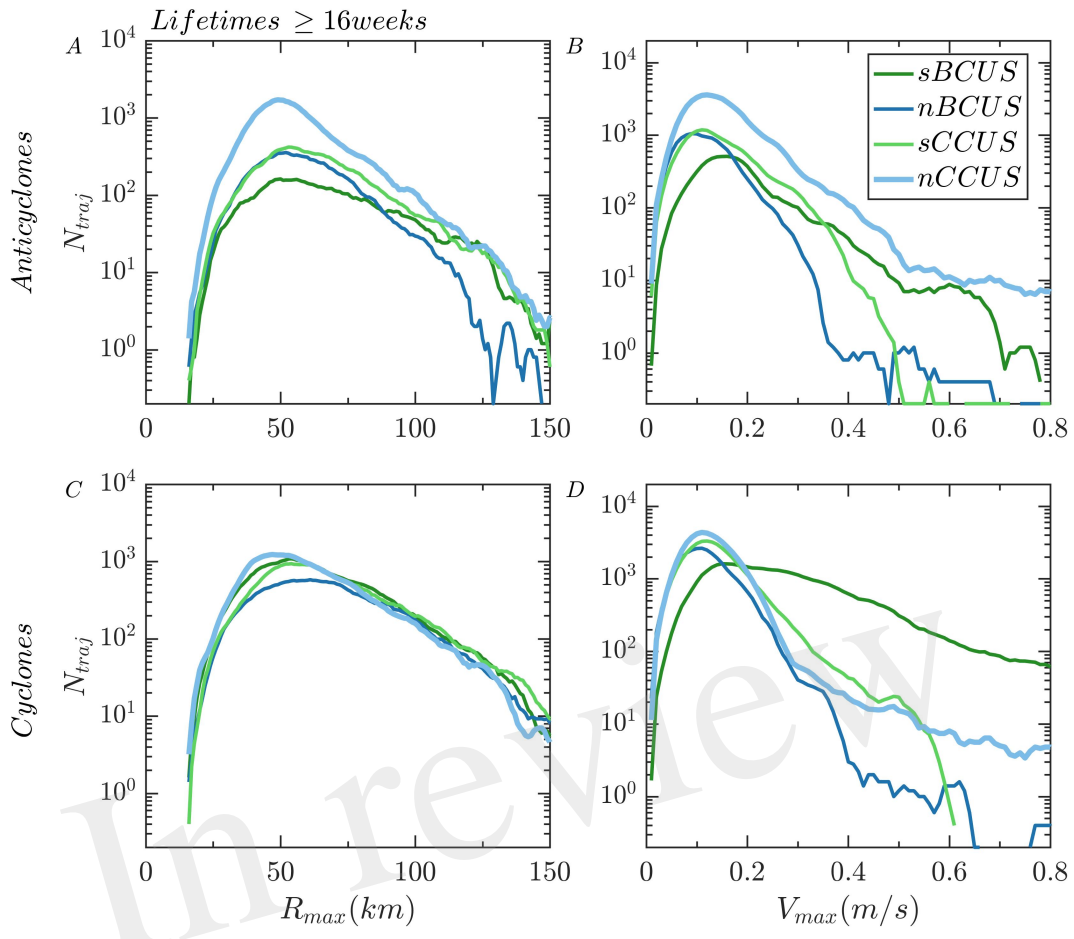


Figure 7. Histograms of eddy characteristic radius R_{max} (km) and velocity V_{max} (m/s) for anticyclonic (panels A and B) and cyclonic trajectories (panels C and D) originating from the different sub-upwelling systems considered in this study (lifetimes ≥ 16 weeks).

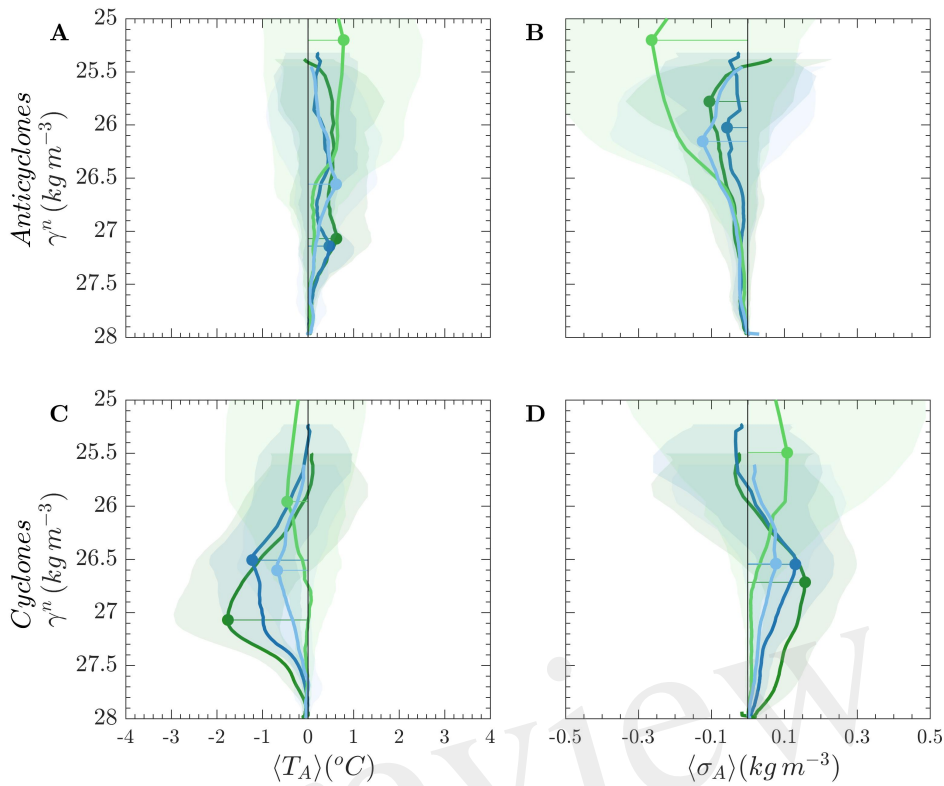


Figure 8. Mean temperature $\langle T_A \rangle$ ($^{\circ}\text{C}$) and density $\langle \sigma_A \rangle$ (kg m^{-3}) anomalies as derived from Argo profiles that were tracked inside anticyclonic (panels A, B and C) and cyclonic trajectories (panels D, E and F) with lifetimes more than ≥ 16 weeks originating from the different sub-upwelling systems considered in this study. Only Argo profiles that were located at a radial distance of less than R_{max} from the estimated eddy center were kept ($d_{argo} \leq R_{max}$).

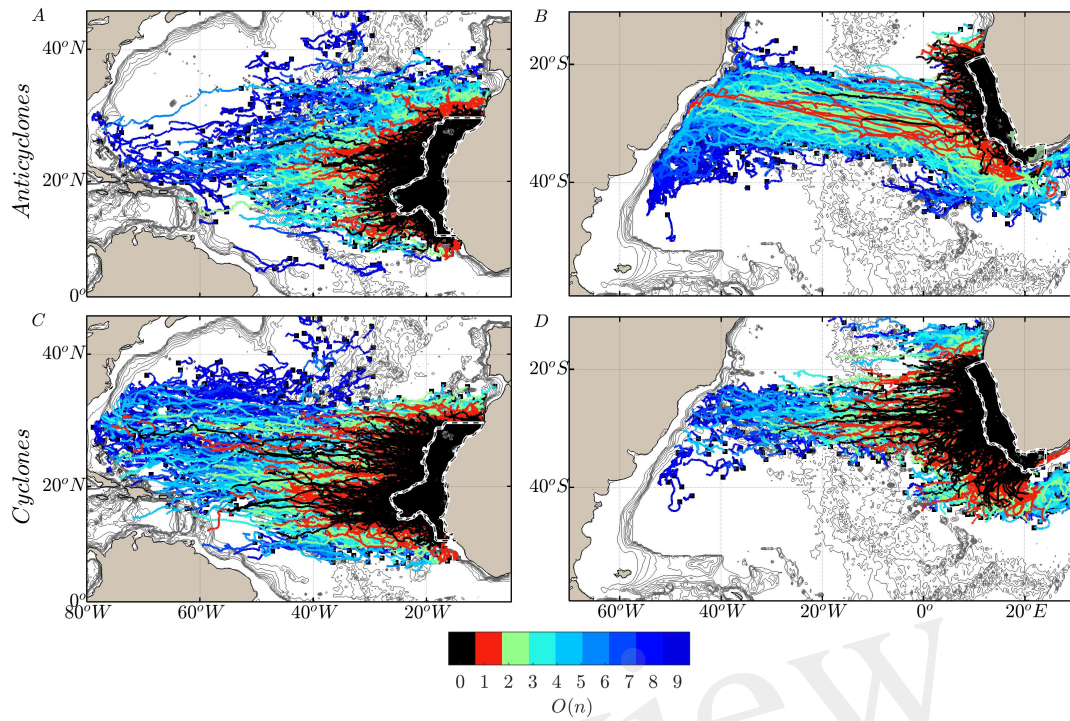


Figure 9. Eddy network of anticyclonic (panels A and B) and cyclonic (panel C and D) trajectories from the CCUS (left panels) and the BCUS (right panels). Each eddy trajectory is colored based on their assigned order. The bathymetry that is shallower than 4000 m is illustrated with the gray lines.

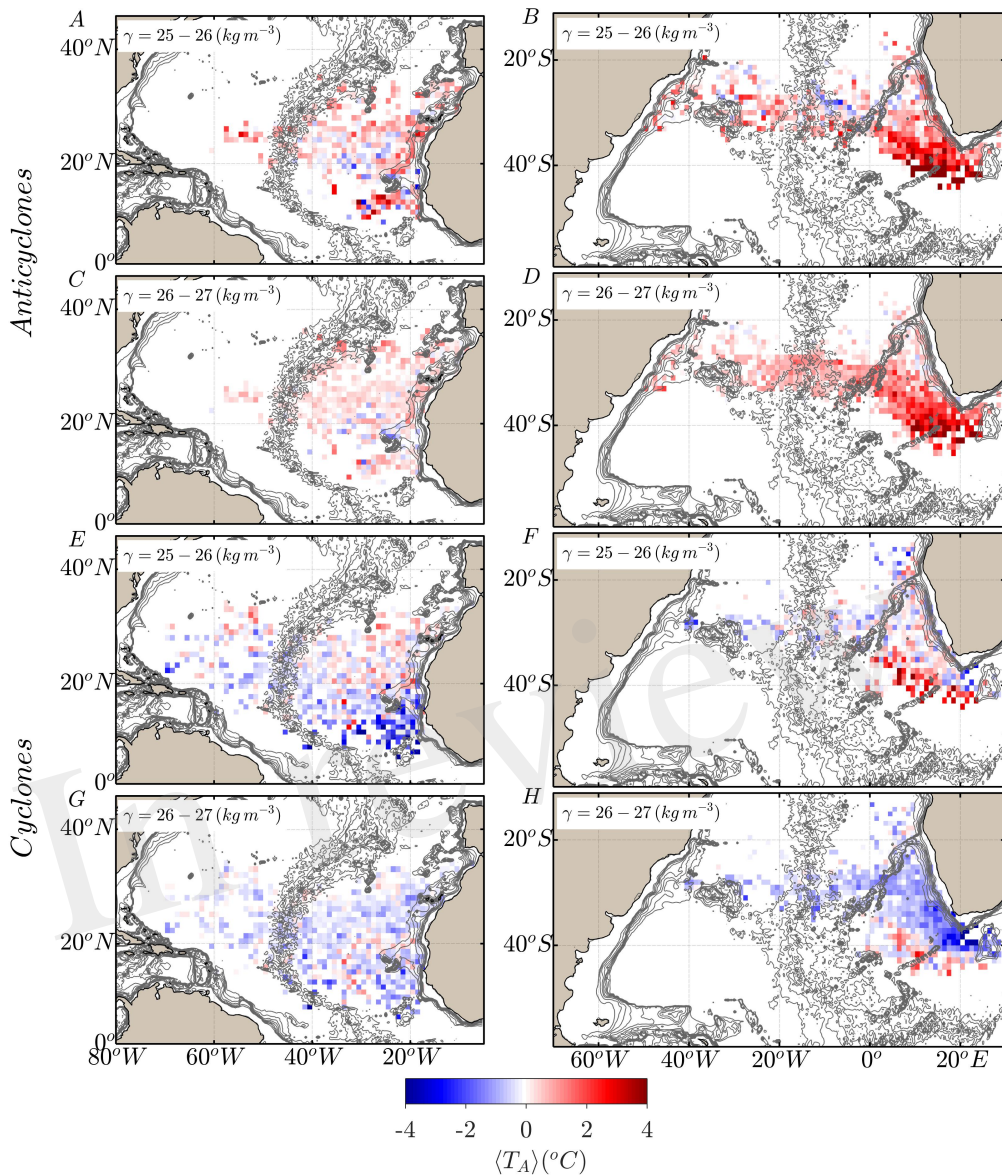


Figure 10. Mean temperature anomalies $\langle T_A \rangle$ ($^{\circ}\text{C}$) at upper ($\gamma = 25 - 26 \text{ kg m}^{-3}$) (A-B and E-F) and deeper ($\gamma = 26 - 27 \text{ kg m}^{-3}$) (C-D and G-H) isopycnal layers as measured by Argo floats trapped inside anticyclones and cyclones from the CCUS (left panels) and the BCUS (right panels) eddy trajectory networks. The bathymetry that is shallower than 4000 m is illustrated with the gray lines.

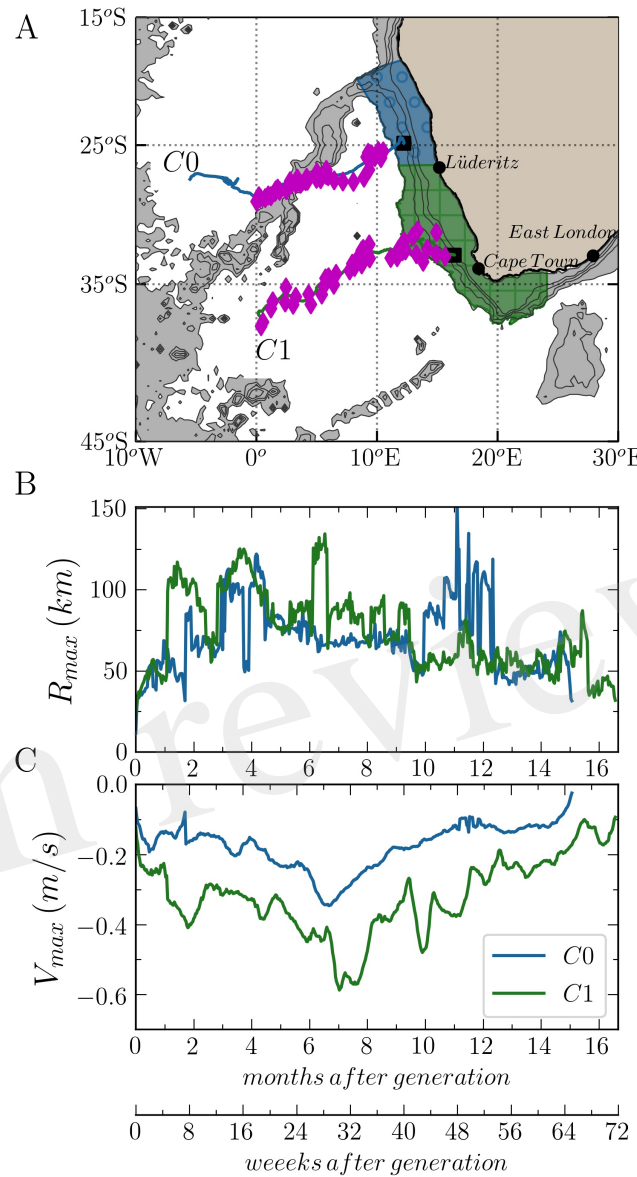


Figure 11. Trajectories of long-lived cyclones C0 and C1 originating from the sBCUS (green patch) and nBCUS (blue patch) as detected from TOEddies database for the years 2012 and 2015 respectively (panel A). The bathymetry that is shallower than 4000 m is illustrated with the gray shading. Temporal evolution of dynamical characteristics of characteristic radius R_{max} (km) and velocity V_{max} (m/s) are shown in B and C.

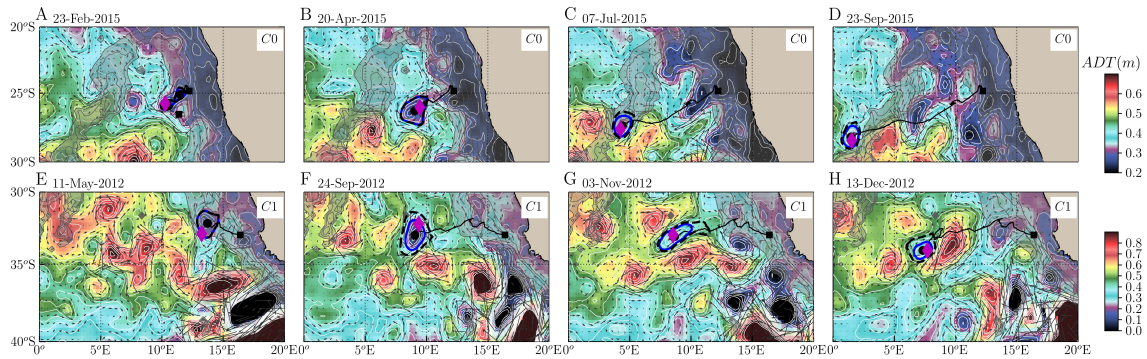


Figure 12. Snapshots along the temporal evolution of the cyclone C0 (panels A-D) and cyclone C1 (panels E-H). The background colors correspond to the ADT while the gray arrows correspond to surface geostrophic velocities. The characteristic and outer contours detected by TOEddies are shown in the blue solid and black dashed lines. The Argo trapped in the eddies are shown with the magenta diamonds points. The bathymetry that is shallower than 4000 m is illustrated with the gray shading.

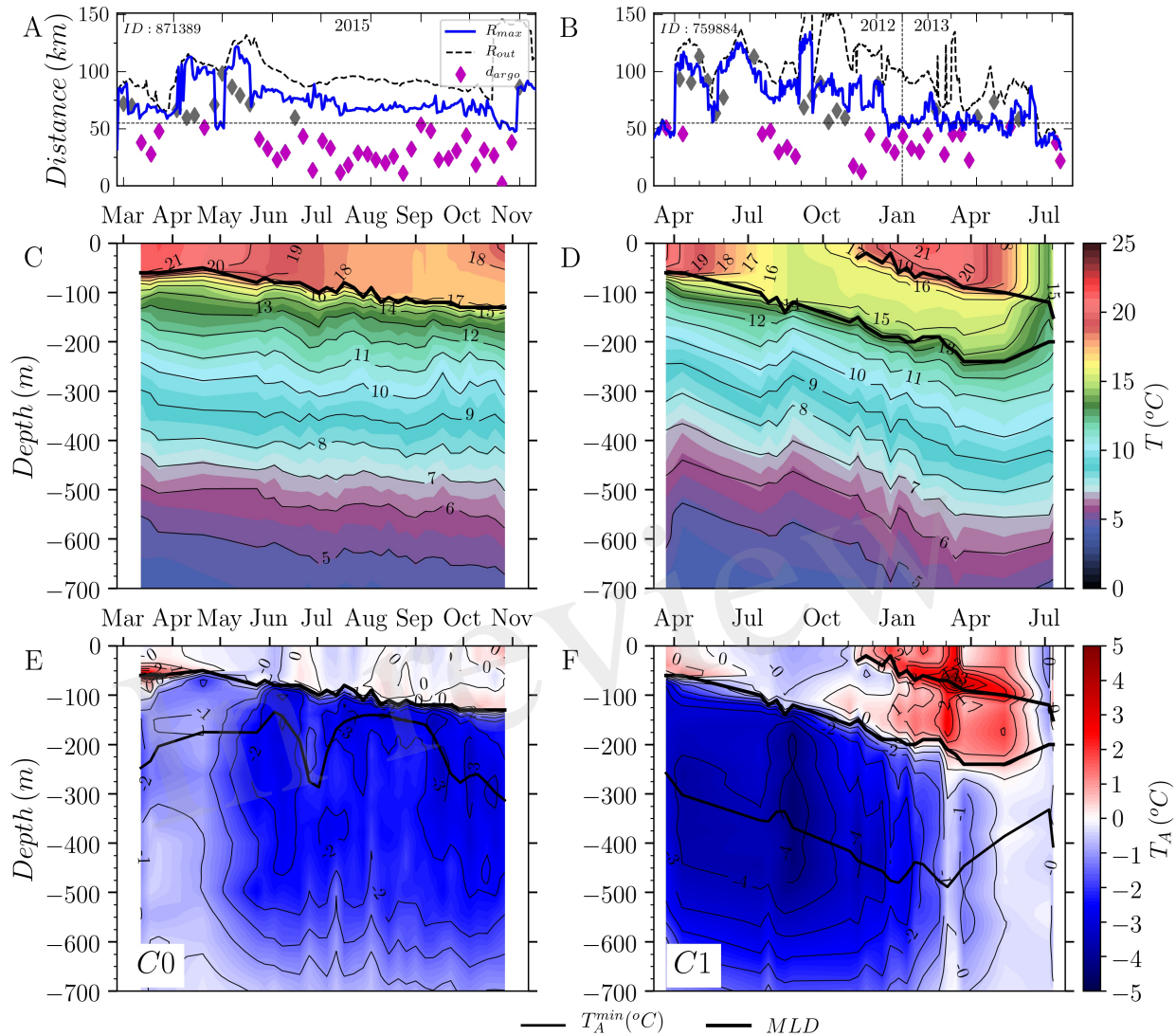


Figure 13. Temporal evolution of eddy characteristic R_{max} (km) and outermost radius R_{out} (km) are shown in panels A and B with the blue and black dashed line for the cyclone C0 and C1 respectively. The diamond magenta points illustrate the position of the Argo profiles as a function of their distance from the eddy center. Vertical profiles of temperature T ($^{\circ}$ C) as obtained from the Argo floats that were trapped in the eddy are shown in panels C and D. The vertical temperature T_A ($^{\circ}$ C) anomalies are shown in panels E and F relative to the TOEddies climatology.

REFERENCES

- 621 Amores, A., Jordà, G., Arsouze, T., and Le Sommer, J. (2018). Up to What Extent Can We Characterize
622 Ocean Eddies Using Present-Day Gridded Altimetric Products? *Journal of Geophysical Research: Oceans* 123, 7220–7236. doi:10.1029/2018JC014140
- 623
- 624 Amos, C. M., Castelao, R. M., and Medeiros, P. M. (2019). Offshore transport of particulate organic
625 carbon in the California Current System by mesoscale eddies. *Nature Communications* 10. doi:10.1038/s41467-019-12783-5
- 626
- 627 Arhan, M., Mercier, H., and Lutjeharms, J. R. E. (1999). The disparate evolution of three Agulhas
628 rings in the South Atlantic Ocean. *Journal of Geophysical Research: Oceans* 104, 20987–21005.
629 doi:10.1029/1998JC900047
- 630 Arhan, M., Speich, S., Messager, C., Dencausse, G., Fine, R., and Boye, M. (2011). Anticyclonic and
631 cyclonic eddies of subtropical origin in the subantarctic zone south of Africa. *Journal of Geophysical
632 Research: Oceans* 116. doi:10.1029/2011JC007140
- 633 Arístegui, J. and Montero, M. F. (2005). Temporal and spatial changes in plankton respiration and biomass
634 in the Canary Islands region: the effect of mesoscale variability. *Journal of Marine Systems* 54, 65–82.
635 doi:10.1016/j.jmarsys.2004.07.004
- 636 Arístegui, J., Sangrà, P., Hernández-León, S., Cantón, M., Hernández-Guerra, A., and Kerling, J. (1994).
637 Island-induced eddies in the Canary Islands. *Deep-Sea Research I* 41, 1509–1525. doi:10.1016/0967-0637(94)90058-2
- 638
- 639 Arístegui, J., Tett, P., Hernández-Guerra, A., Basterretxea, G., Montero, M., Wild, K., et al. (1997). The
640 influence of island-generated eddies on chlorophyll distribution: a study of mesoscale variation around
641 Gran Canaria. *Deep-Sea Research I* 44, 71–96. doi:10.1016/s0967-0637(96)00093-3
- 642 Assassi, C., Morel, Y., Vandermeirsch, F., Chaigneau, A., Pegliasco, C., Morrow, R., et al. (2016). An
643 Index to Distinguish Surface- and Subsurface-Intensified Vortices from Surface Observations. *Journal
644 of Physical Oceanography* 46, 2529–2552. doi:10.1175/JPO-D-15-0122.1
- 645 Barceló-Llull, B., Sangrà, P., Pallàs-Sanz, E., Barton, E. D., Estrada-Allis, S. N., Martínez-Marrero, A.,
646 et al. (2017). Anatomy of a subtropical intrathermocline eddy. *Deep Sea Research Part I: Oceanographic
647 Research Papers* 124, 126–139. doi:10.1016/j.dsr.2017.03.012
- 648 Barton, E., Arístegui, J., Tett, P., Cantón, M., García-Braun, J., Hernández-León, S., et al. (1998). The
649 transition zone of the Canary Current upwelling region. *Progress in Oceanography* 41, 455–504.
650 doi:10.1016/S0079-6611(98)00023-8
- 651 Barton, E. D., Arístegui, J., Tett, P., and Pérez, E. N. (2004). Variability in the Canary Islands area of
652 filament-eddy exchanges. *Progress in Oceanography* 62, 71–94. doi:10.1016/j.pocean.2004.07.003
- 653 Basterretxea, G., Barton, E., Tett, P., Sangrà, P., Navarro-Perez, E., and Arístegui, J. (2002). Eddy
654 and deep chlorophyl maximum response to wind-shear in the lee of Gran Canaria 49, 1087–1101.
655 doi:10.1016/S0967-0637(02)00009-2
- 656 Benazzouz, A., Mordane, S., Orbi, A., Chagdali, M., Hilmi, K., Atillah, A., et al. (2014). An improved
657 coastal upwelling index from sea surface temperature using satellite-based approach – The case of the
658 Canary Current upwelling system. *Continental Shelf Research* 81, 38–54. doi:10.1016/j.csr.2014.03.012
- 659 Blamey, L. K., Shannon, L. J., Bolton, J. J., Crawford, R. J., Dufois, F., Evers-King, H., et al. (2015).
660 Ecosystem change in the southern Benguela and the underlying processes. *Journal of Marine Systems*
661 144, 9–29. doi:10.1016/j.jmarsys.2014.11.006
- 662 Blanke, B., Penven, P., Roy, C., Chang, N., and Kokoszka, F. (2009). Ocean variability over the Agulhas
663 Bank and its dynamical connection with the southern Benguela upwelling system. *Journal of Geophysical
664 Research* 114. doi:10.1029/2009JC005358

- 665 Boebel, O., Lutjeharms, J., Schmid, C., Zenk, W., Rossby, T., and Barron, C. (2003). The cape cauldron: a
666 regime of turbulent inter-ocean exchange. *Deep Sea Research Part II: Topical Studies in Oceanography*
667 50, 57–86. doi:10.1016/s0967-0645(02)00379-x
- 668 Brandt, P., Bange, H. W., Banyte, D., Dengler, M., Didwischus, S.-H., Fischer, T., et al. (2015). On the
669 role of circulation and mixing in the ventilation of oxygen minimum zones with a focus on the eastern
670 tropical North Atlantic. *Biogeosciences* 12, 489–512. doi:10.5194/bg-12-489-2015
- 671 Caldeira, R. M. A., Stegner, A., Couvelard, X., Araújo, I. B., Testor, P., and Lorenzo, A. (2014). Evolution
672 of an oceanic anticyclone in the lee of Madeira Island: In situ and remote sensing survey. *Journal of*
673 *Geophysical Research: Oceans* 119, 1195–1216. doi:10.1002/2013jc009493
- 674 Chaigneau, A., Eldin, G., and Dewitte, B. (2009). Eddy activity in the four major upwelling systems from
675 satellite altimetry (1992–2007). *Progress in Oceanography* 83, 117–123. doi:10.1016/j.pocean.2009.07.
676 012
- 677 Chaigneau, A., Le Texier, M., Eldin, G., Grados, C., and Pizarro, O. (2011). Vertical structure of mesoscale
678 eddies in the eastern South Pacific Ocean: A composite analysis from altimetry and Argo profiling floats.
679 *Journal of Geophysical Research: Oceans* 116, 1–16. doi:10.1029/2011JC007134
- 680 Chelton, D. B., Schlax, M. G., and Samelson, R. M. (2011). Global observations of nonlinear mesoscale
681 eddies. *Progress in Oceanography* 91, 167–216. doi:10.1016/j.pocean.2011.01.002
- 682 Cornec, M., Claustre, H., Mignot, A., Guidi, L., Lacour, L., Poteau, A., et al. (2021a). Deep Chlorophyll
683 Maxima in the Global Ocean: Occurrences, Drivers and Characteristics. *Global Biogeochemical Cycles*
684 35. doi:10.1029/2020gb006759
- 685 Cornec, M., Laxenaire, R., Speich, S., and Claustre, H. (2021b). Impact of Mesoscale Eddies on Deep
686 Chlorophyll Maxima. *Geophysical Research Letters* 48. doi:10.1029/2021gl093470
- 687 Correa-Ramirez, M. A., Hormazábal, S., and Yuras, G. (2007). Mesoscale eddies and high chlorophyll
688 concentrations off central Chile (29°–39°S). *Geophysical Research Letters* 34. doi:10.1029/
689 2007GL029541
- 690 Cui, W., Wang, W., Zhang, J., and Yang, J. (2019). Multicore structures and the splitting and merging
691 of eddies in global oceans from satellite altimeter data. *Ocean Science* 15, 413–430. doi:10.5194/
692 os-15-413-2019
- 693 Cury, P. and Shannon, L. (2004). Regime shifts in upwelling ecosystems: observed changes and possible
694 mechanisms in the northern and southern Benguela. *Progress in Oceanography* 60, 223–243. doi:10.
695 1016/j.pocean.2004.02.007
- 696 de Marez, C., L'Hégaret, P., Morvan, M., and Carton, X. (2019). On the 3D structure of eddies in the
697 Arabian Sea. *Deep Sea Research Part I: Oceanographic Research Papers* 150, 103057. doi:10.1016/j.
698 dsr.2019.06.003
- 699 Desbiolles, F., Blanke, B., Bentamy, A., and Grima, N. (2014). Origin of fine-scale wind stress curl
700 structures in the Benguela and Canary upwelling systems. *Journal of Geophysical Research: Oceans*
701 119, 7931–7948. doi:10.1002/2014JC010015
- 702 Dilmahamod, A. F., Aguiar-González, B., Penven, P., Reason, C. J. C., Ruijter, W. P. M. D., Malan, N.,
703 et al. (2018). SIDDIES Corridor: A Major East-West Pathway of Long-Lived Surface and Subsurface
704 Eddies Crossing the Subtropical South Indian Ocean. *Journal of Geophysical Research: Oceans* 123,
705 5406–5425. doi:10.1029/2018jc013828
- 706 Dilmahamod, A. F., Karstensen, J., Dietze, H., Löptien, U., and Fennel, K. (2021). Generation mechanisms
707 of mesoscale eddies in the Mauritanian Upwelling Region. *Journal of Physical Oceanography* doi:10.
708 1175/jpo-d-21-0092.1

- 709 Doglioli, A., Blanke, B., Speich, S., and Lapeyre, G. (2007). Tracking coherent structures in a regional
710 ocean model with wavelet analysis: Application to Cape Basin Eddies. *Journal of Geophysical Research*
711 112. doi:10.1029/2006jc003952
- 712 Du, Y., Yi, J., Wu, D., He, Z., Wang, D., and Fuyuan, L. (2014). Mesoscale oceanic eddies in the South
713 China Sea from 1992 to 2012: evolution processes and statistical analysis. *Acta Oceanologica Sinica* 33,
714 36–47. doi:10.1007/s13131-014-0530-6
- 715 Dufois, F., Hardman-Mountford, N. J., Greenwood, J., Richardson, A. J., Feng, M., and Matear, R. J.
716 (2016). Anticyclonic eddies are more productive than cyclonic eddies in subtropical gyres because of
717 winter mixing. *Science Advances* 2, e1600282. doi:10.1126/sciadv.1600282
- 718 Duncombe Rae, C., Shillington, F., Agenbag, J., Taunton-Clark, J., and Gründlingh, M. (1992). An Agulhas
719 ring in the South Atlantic Ocean and its interaction with the Benguela upwelling frontal system. *Deep Sea*
720 *Research Part A: Oceanographic Research Papers* 39, 2009–2027. doi:10.1016/0198-0149(92)90011-H
- 721 Flierl, G. R. (1981). Particle motions in large-amplitude wave fields. *Geophysical & Astrophysical Fluid*
722 *Dynamics* 18, 39–74. doi:10.1080/03091928108208773
- 723 Giulivi, C. F. and Gordon, A. L. (2006). Isopycnal displacements within the Cape Basin thermocline as
724 revealed by the Hydrographic Data Archive. *Deep Sea Research Part I: Oceanographic Research Papers* 53,
725 1285–1300. doi:10.1016/j.dsr.2006.05.011
- 726 Gruber, N., Lachkar, Z., Frenzel, H., Marchesiello, P., Münnich, M., McWilliams, J. C., et al. (2011). Eddy-
727 induced reduction of biological production in eastern boundary upwelling systems. *Nature Geoscience*
728 4, 787–792. doi:10.1038/ngeo1273
- 729 Guerra, L. A. A., Paiva, A. M., and Chassignet, E. P. (2018). On the translation of Agulhas rings to
730 the western South Atlantic Ocean. *Deep Sea Research Part I: Oceanographic Research Papers* 139,
731 104–113. doi:10.1016/j.dsr.2018.08.005
- 732 Harvey, C. J., Fisher, J. L., Samhouri, J. F., Williams, G. D., Francis, T. B., Jacobson, K. C., et al.
733 (2020). The importance of long-term ecological time series for integrated ecosystem assessment and
734 ecosystem-based management. *Progress in Oceanography* 188, 102418. doi:<https://doi.org/10.1016/j.pocean.2020.102418>
- 735 Hersbach, H., Bell, B., Berrisford, P., Biavati, G., Horányi, A., Muñoz Sabater, J., et al. (2018). ERA5
736 hourly data on single levels from 1979 to present. Copernicus Climate Change Service (C3S) Climate
737 Data Store (CDS) doi:10.24381/cds.adbb2d47
- 738 Hutchings, L., van der Lingen, C., Shannon, L., Crawford, R., Verheyen, H., Bartholomae, C., et al. (2009).
739 The Benguela Current: An ecosystem of four components. *Progress in Oceanography* 83, 15–32.
740 doi:10.1016/j.pocean.2009.07.046
- 741 Ioannou, A., Stegner, A., Dubos, T., Le Vu, B., and Speich, S. (2020a). Generation and Intensification of
742 Mesoscale Anticyclones by Orographic Wind Jets: The Case of Ierapetra Eddies Forced by the Etesians.
743 *Journal of Geophysical Research: Oceans* 125, e2019JC015810. doi:10.1029/2019jc015810
- 744 Ioannou, A., Stegner, A., Dumas, F., and Vu, B. L. (2020b). Three-Dimensional Evolution of Mesoscale
745 Anticyclones in the Lee of Crete. *Frontiers in Marine Science* 7. doi:10.3389/fmars.2020.609156
- 746 Ioannou, A., Stegner, A., Le Vu, B., Taupier-Letage, I., and Speich, S. (2017). Dynamical Evolution of
747 Intense Ierapetra Eddies on a 22 Year Long Period. *Journal of Geophysical Research: Oceans* 122,
748 9276–9298. doi:10.1002/2017jc013158
- 749 Karstensen, J., Schütte, F., Pietri, A., Krahmann, G., Fiedler, B., Grundle, D., et al. (2017). Upwelling
750 and isolation in oxygen-depleted anticyclonic modewater eddies and implications for nitrate cycling.
751 *Biogeosciences* 14, 2167–2181. doi:10.5194/bg-14-2167-2017

- 753 Kirkman, S., Blamey, L., Lamont, T., Field, J., Bianchi, G., Huggett, J., et al. (2016). Spatial
754 characterisation of the Benguela ecosystem for ecosystem-based management. *African Journal of
755 Marine Science* 38, 7–22. doi:10.2989/1814232X.2015.1125390
- 756 Laxenaire, R., Speich, S., Blanke, B., Chaigneau, A., Pegliasco, C., and Stegner, A. (2018). Anticyclonic
757 Eddies Connecting the Western Boundaries of Indian and Atlantic Oceans. *Journal of Geophysical
758 Research: Oceans* 123, 7651–7677. doi:10.1029/2018JC014270
- 759 Laxenaire, R., Speich, S., and Stegner, A. (2019). Evolution of the Thermohaline Structure of One Agulhas
760 Ring Reconstructed from Satellite Altimetry and Argo Floats. *Journal of Geophysical Research* 124,
761 8969–9003. doi:10.1029/2018jc014426
- 762 Laxenaire, R., Speich, S., and Stegner, A. (2020). Agulhas Ring Heat Content and Transport in the
763 South Atlantic Estimated by Combining Satellite Altimetry and Argo Profiling Floats Data. *Journal of
764 Geophysical Research: Oceans* 125. doi:10.1029/2019jc015511
- 765 Lehahn, Y., d’Ovidio, F., Lévy, M., Amitai, Y., and Heifetz, E. (2011). Long range transport of a
766 quasi isolated chlorophyll patch by an Agulhas ring. *Geophysical Research Letters* 38. doi:10.1029/
767 2011GL048588
- 768 Le Vu, B., Stegner, A., and Arsouze, T. (2018). Angular Momentum Eddy Detection and Tracking
769 Algorithm (AMEDA) and Its Application to Coastal Eddy Formation. *Journal of Atmospheric and
770 Oceanic Technology* 35, 739–762. doi:10.1175/jtech-d-17-0010.1
- 771 Li, Q.-Y., Sun, L., Liu, S.-S., Xian, T., and Yan, Y.-F. (2014). A new mononuclear eddy identification
772 method with simple splitting strategies. *Remote Sensing Letters* 5, 65–72. doi:10.1080/2150704X.2013.
773 872814
- 774 Luko, C. D., Silveira, I. C. A., Simoes-Sousa, I. T., Araujo, J. M., and Tandon, A. (2021). Revisiting
775 the Atlantic South Equatorial Current. *Journal of Geophysical Research: Oceans* 126. doi:10.1029/
776 2021jc017387
- 777 Lumpkin, R. (2016). Global characteristics of coherent vortices from surface drifter trajectories. *Journal
778 of Geophysical Research: Oceans* 121, 1306–1321. doi:10.1002/2015jc011435
- 779 Majumder, S., Goes, M., Polito, P. S., Lumpkin, R., Schmid, C., and Lopez, H. (2019). Propagating Modes
780 of Variability and Their Impact on the Western Boundary Current in the South Atlantic. *Journal of
781 Geophysical Research: Oceans* 124, 3168–3185. doi:10.1029/2018jc014812
- 782 Manta, G., Speich, S., Karstensen, J., Hummels, R., Kersalé, M., Laxenaire, R., et al. (2021). The South
783 Atlantic Meridional Overturning Circulation and Mesoscale Eddies in the First GO-SHIP Section at
784 34.5°S. *Journal of Geophysical Research: Oceans* 126. doi:10.1029/2020JC016962
- 785 Marchesiello, P. and Estrade, P. (2007). Eddy activity and mixing in upwelling systems: a comparative
786 study of Northwest Africa and California regions. *International Journal of Earth Sciences* 98, 299–308.
787 doi:10.1007/s00531-007-0235-6
- 788 Marchesiello, P., McWilliams, J. C., and Shchepetkin, A. (2003). Equilibrium structure and dynamics
789 of the California current system. *Journal of Physical Oceanography* 33, 753–783. doi:10.1175/
790 1520-0485(2003)33<753:esadot>2.0.co;2
- 791 Matano, R. and Beier, E. (2003). A kinematic analysis of the Indian/Atlantic interocean exchange. *Deep Sea
792 Research Part II: Topical Studies in Oceanography* 50, 229–249. doi:10.1016/s0967-0645(02)00395-8
- 793 McDougall, T. J. and Barker, P. M. (2011). *Getting started with TEOS-10 and the Gibbs Seawater (GSW)*
794 *Oceanographic Toolbox*
- 795 McGillicuddy, D. J., Anderson, L. A., Bates, N. R., Bibby, T., Buesseler, K. O., Carlson, C. A., et al.
796 (2007). Eddy/Wind Interactions Stimulate Extraordinary Mid-Ocean Plankton Blooms. *Science* 316,
797 1021–1026. doi:10.1126/science.1136256

- 798 Morrow, R. (2004). Divergent pathways of cyclonic and anti-cyclonic ocean eddies. *Geophysical Research
799 Letters* 31. doi:10.1029/2004gl020974
- 800 Moscoso, J. E., Stewart, A. L., Bianchi, D., and McWilliams, J. C. (2021). The meridionally averaged
801 model of eastern boundary upwelling systems (MAMEBUSv1.0). *Geoscientific Model Development* 14,
802 763–794. doi:10.5194/gmd-14-763-2021
- 803 Nagai, T., Gruber, N., Frenzel, H., Lachkar, Z., McWilliams, J. C., and Plattner, G.-K. (2015). Dominant
804 role of eddies and filaments in the offshore transport of carbon and nutrients in the California Current
805 Systems. *Journal of Geophysical Research: Oceans* 120, 5318–5341. doi:10.1002/2015JC010889
- 806 Ndoye, S., Capet, X., Estrade, P., Sow, B., Dagorne, D., Lazar, A., et al. (2014). SST patterns and dynamics
807 of the southern Senegal-Gambia upwelling center. *Journal of Geophysical Research: Oceans* 119,
808 8315–8335. doi:10.1002/2014jc010242
- 809 Nencioli, F., Olmo, G. D., and Quartly, G. D. (2018). Agulhas Ring Transport Efficiency From Combined
810 Satellite Altimetry and Argo Profiles 123, 5874–5888. doi:10.1029/2018JC013909
- 811 Pegliasco, C., Chaigneau, A., and Morrow, R. (2015). Main eddy vertical structures observed in the four
812 major Eastern Boundary Upwelling Systems. *Journal of Geophysical Research: Oceans* 120, 6008–6033.
813 doi:10.1002/2015JC010950
- 814 Pegliasco, C., Chaigneau, A., Morrow, R., and Dumas, F. (2020). Detection and tracking of mesoscale
815 eddies in the Mediterranean Sea: A comparison between the Sea Level Anomaly and the Absolute
816 Dynamic Topography fields. *Advances in Space Research* doi:10.1016/j.asr.2020.03.039
- 817 Pelegrí, J. L. and Benazzouz, A. (2015). Coastal upwelling off North-West Africa
- 818 Polito, P. S. and Sato, O. T. (2015). Do eddies ride on Rossby waves? *Journal of Geophysical Research:
819 Oceans* 120, 5417–5435. doi:10.1002/2015jc010737
- 820 Richardson, P. and Garzoli, S. (2003). Characteristics of intermediate water flow in the Benguela current as
821 measured with RAFOS floats. *Deep-Sea Research II* 50, 87–118. doi:10.1016/S0967-0645(02)00380-6
- 822 Rusciano, E., Speich, S., and Ollitrault, M. (2012). Intercean exchanges and the spreading of Antarctic
823 Intermediate Water south of Africa. *Journal of Geophysical Research: Oceans* 117, n/a–n/a. doi:10.
824 1029/2012JC008266
- 825 Sangrà, P., Auladell, M., Marrero-Díaz, A., Pelegrí, J., Fraile-Nuez, E., Rodríguez-Santana, A., et al.
826 (2007). On the nature of oceanic eddies shed by the Island of Gran Canaria. *Deep-Sea Research I* 54,
827 687–709. doi:10.1016/j.dsr.2007.02.004
- 828 Sangrà, P., Pascual, A., Rodríguez-Santana, Á., Machín, F., Mason, E., McWilliams, J. C., et al. (2009). The
829 Canary Eddy Corridor: A major pathway for long-lived eddies in the subtropical North Atlantic. *Deep
830 Sea Research Part I: Oceanographic Research Papers* 56, 2100–2114. doi:10.1016/j.dsr.2009.08.008
- 831 Sangrà, P., Pelegrí, J. L., Hernández-Guerra, A., Arregui, I., Martín, J. M., Marrero-Díaz, A., et al. (2005).
832 Life history of an anticyclonic eddy. *Journal of Geophysical Research* 110. doi:10.1029/2004JC002526
- 833 Schütte, F., Brandt, P., and Karstensen, J. (2016a). Occurrence and characteristics of mesoscale eddies in
834 the tropical northeastern Atlantic Ocean. *Ocean Science* 12, 663–685. doi:10.5194/os-12-663-2016
- 835 Schütte, F., Karstensen, J., Krahmann, G., Hauss, H., Fiedler, B., Brandt, P., et al. (2016b). Characterization
836 of 'dead-zone' eddies in the eastern tropical North Atlantic. *Biogeosciences* 13, 5865–5881. doi:10.
837 5194/bg-13-5865-2016
- 838 Souza, J. M. A., de Boyer Montégut, C., and Traon, P.-Y. L. (2011). Comparison between three
839 implementations of automatic identification algorithms for the quantification and characterization of
840 mesoscale eddies in the South Atlantic Ocean. *Ocean Sci.* 7, 317–334
- 841 Stegner, A. (2014). Oceanic Island Wake Flows in the Laboratory, in Modeling Atmospheric and Oceanic
842 Flows: Insights from Laboratory Experiments and Numerical Simulations. *Remote Sensing Letters* ,

- 843 265–276doi:10.1080/2150704X.2013.872814
- 844 Stegner, A., Vu, B. L., Dumas, F., Ghannami, M. A., Nicolle, A., Durand, C., et al. (2021). Cyclone-
845 Anticyclone Asymmetry of Eddy Detection on Gridded Altimetry Product in the Mediterranean Sea.
846 *Journal of Geophysical Research: Oceans* 126. doi:10.1029/2021JC017475
- 847 Stevens, B., Bony, S., Farrell, D., Ament, F., Blyth, A., Fairall, C., et al. (2021). EUREC⁴A. *Earth System
848 Science Data* 13, 4067–4119. doi:10.5194/essd-13-4067-2021
- 849 Stramma, L., Bange, H. W., Czeschel, R., Lorenzo, A., and Frank, M. (2013). On the role of mesoscale
850 eddies for the biological productivity and biogeochemistry in the eastern tropical Pacific Ocean off Peru.
851 *Biogeosciences* 10, 7293–7306. doi:10.5194/bg-10-7293-2013
- 852 Tian, F., Wu, D., Yuan, L., and Chen, G. (2019). Impacts of the efficiencies of identification and
853 tracking algorithms on the statistical properties of global mesoscale eddies using merged altimeter data.
854 *International Journal of Remote Sensing* 41, 2835–2860. doi:10.1080/01431161.2019.1694724
- 855 Veitch, J. A. and Penven, P. (2017). The role of the Agulhas in the Benguela Current system:
856 A numerical modeling approach. *Journal of Geophysical Research: Oceans* 122, 3375–3393.
857 doi:10.1002/2016JC012247
- 858 Villar, E., Farrant, G. K., Follows, M., Garczarek, L., Speich, S., Audic, S., et al. (2015). Ocean plankton.
859 Environmental characteristics of Agulhas rings affect interocean plankton transport. *Science* 348,
860 1261447–1261447. doi:10.1126/science.1261447
- 861 Wang, Y., Castelao, R. M., and Yuan, Y. (2015). Seasonal variability of alongshore winds and sea surface
862 temperature fronts in eastern boundary current systems. *Journal of Geophysical Research: Oceans* 120,
863 2385–2400. doi:10.1002/2014jc010379
- 864 Wang, Y., Liu, J., Liu, H., Lin, P., Yuan, Y., and Chai, F. (2021). Seasonal and interannual variability in the
865 sea surface temperature front in the eastern pacific ocean. *Journal of Geophysical Research: Oceans*
866 126. doi:10.1029/2020jc016356
- 867 Wang, Y., Zhang, H.-R., Chai, F., and Yuan, Y. (2018). Impact of mesoscale eddies on chlorophyll
868 variability off the coast of chile. *PLOS ONE* 13, e0203598. doi:10.1371/journal.pone.0203598

Figure 1.JPEG

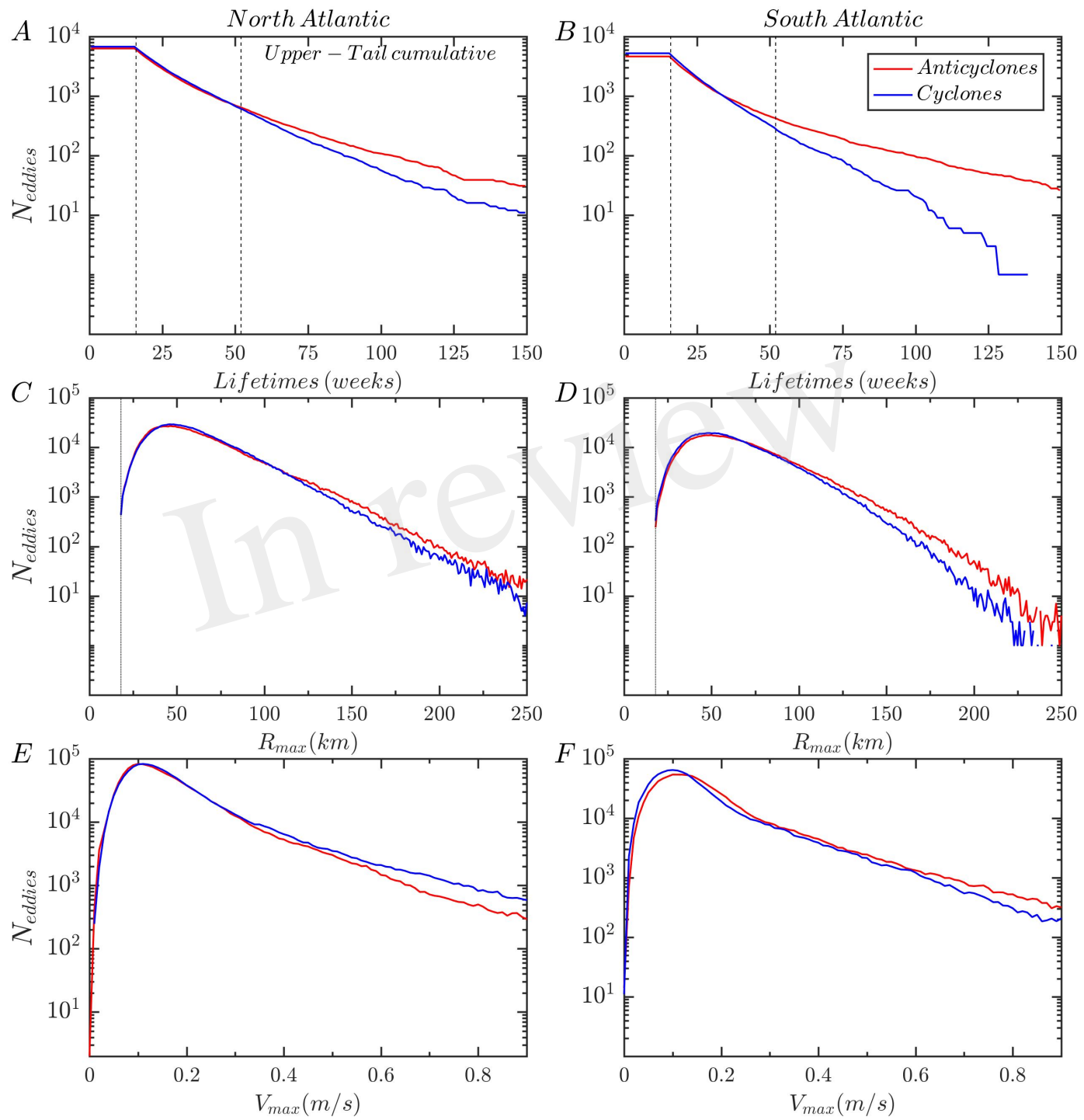


Figure 2.JPEG

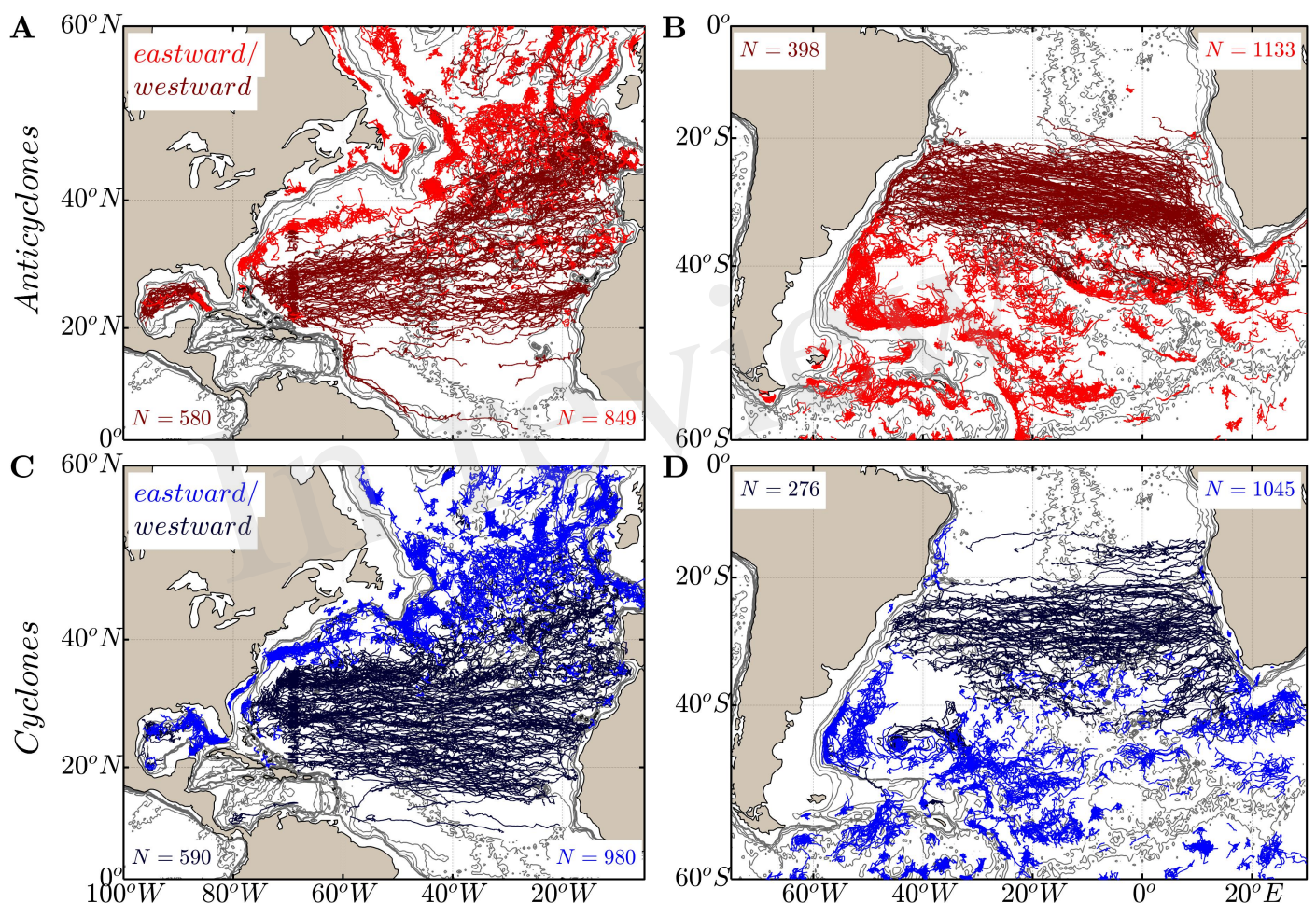


Figure 3.JPEG

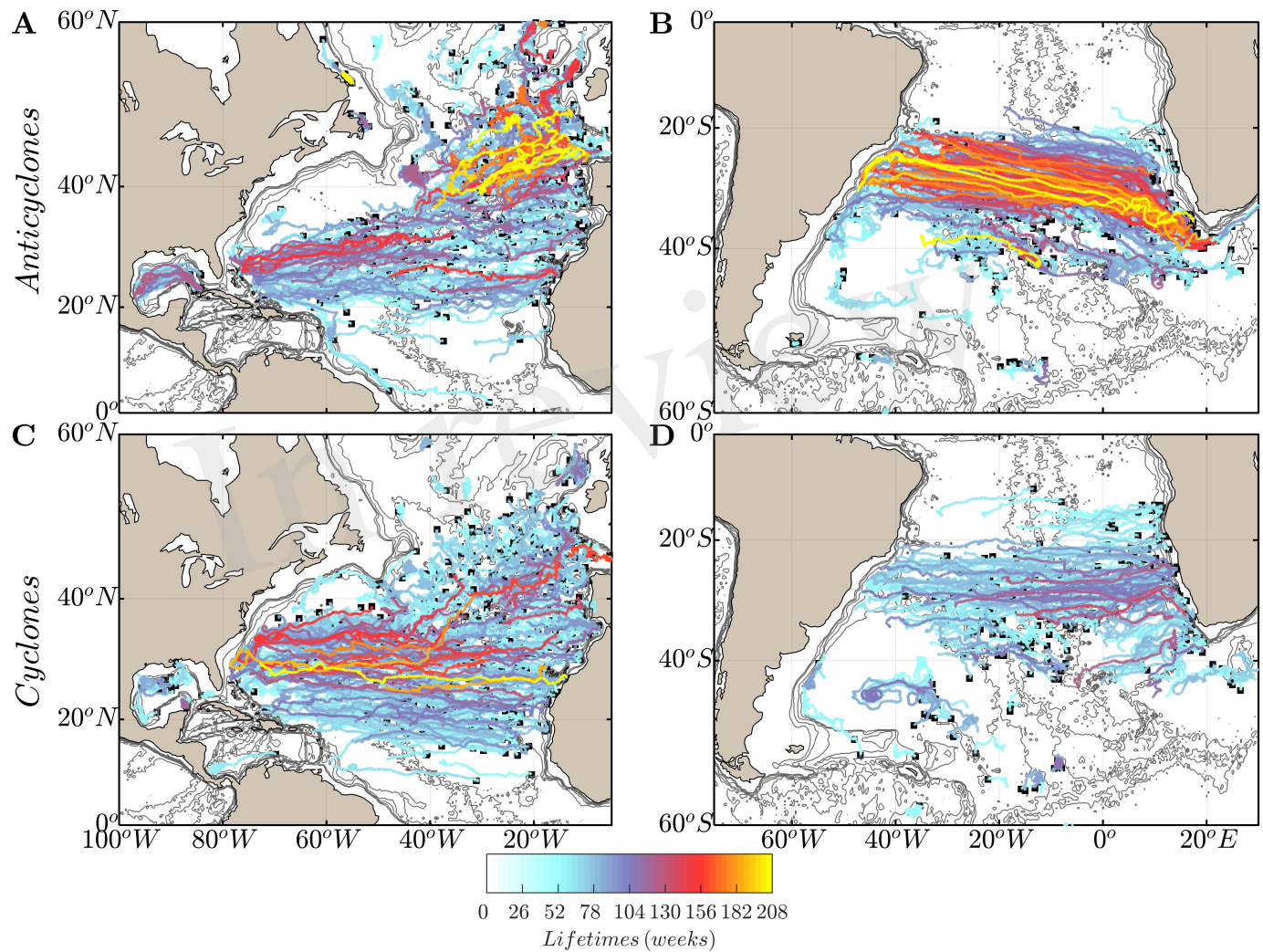


Figure 4.JPEG

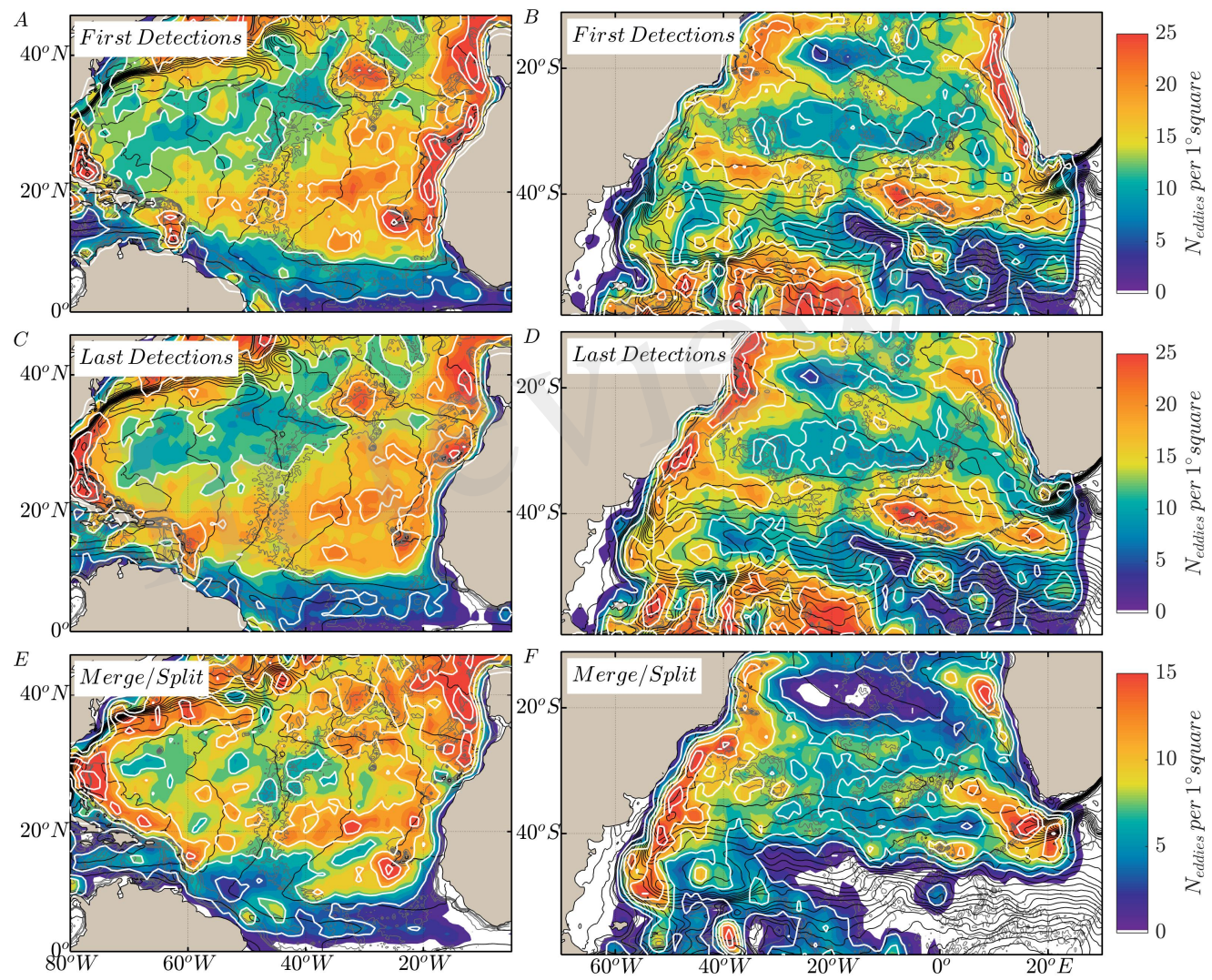


Figure 5.JPEG

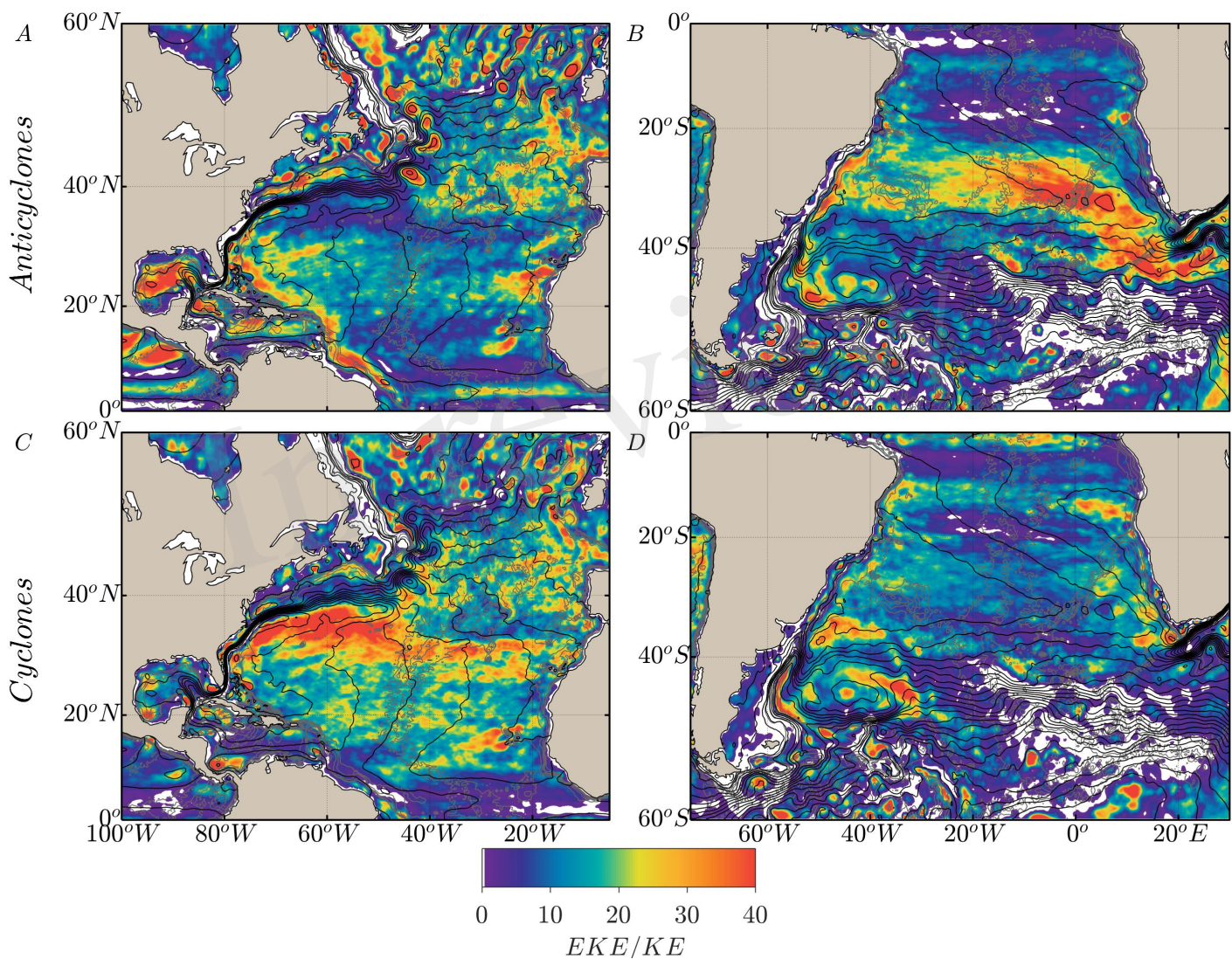


Figure 6.JPG

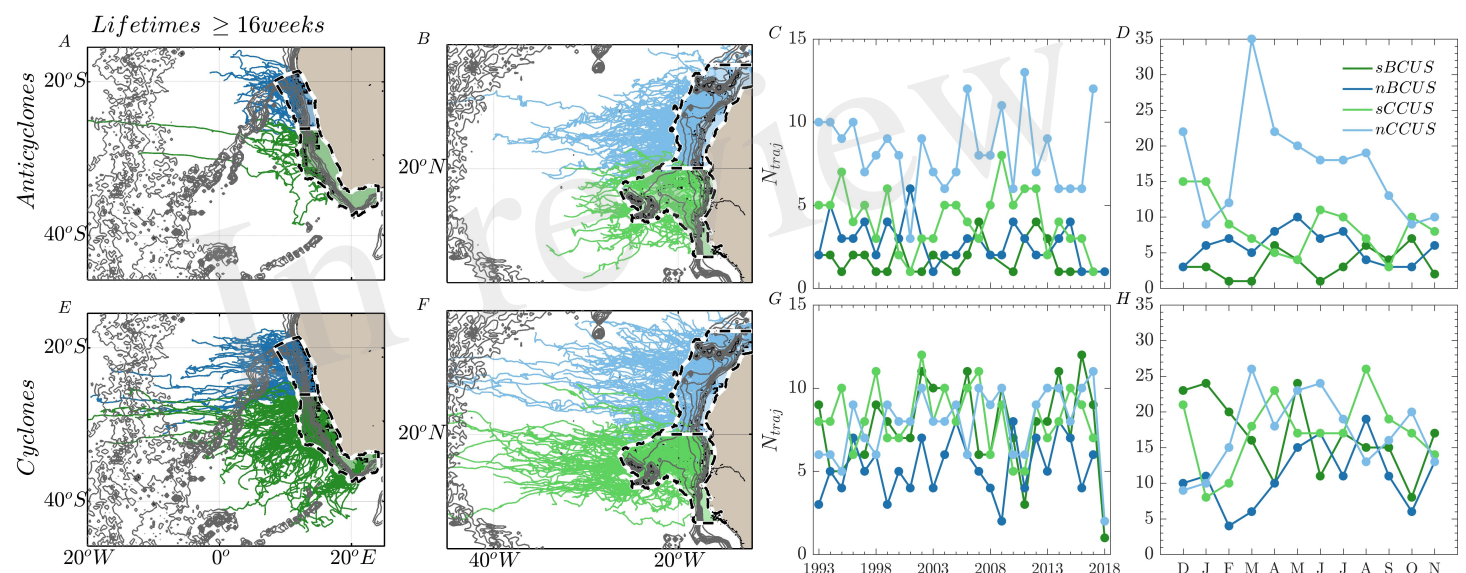


Figure 7.JPG

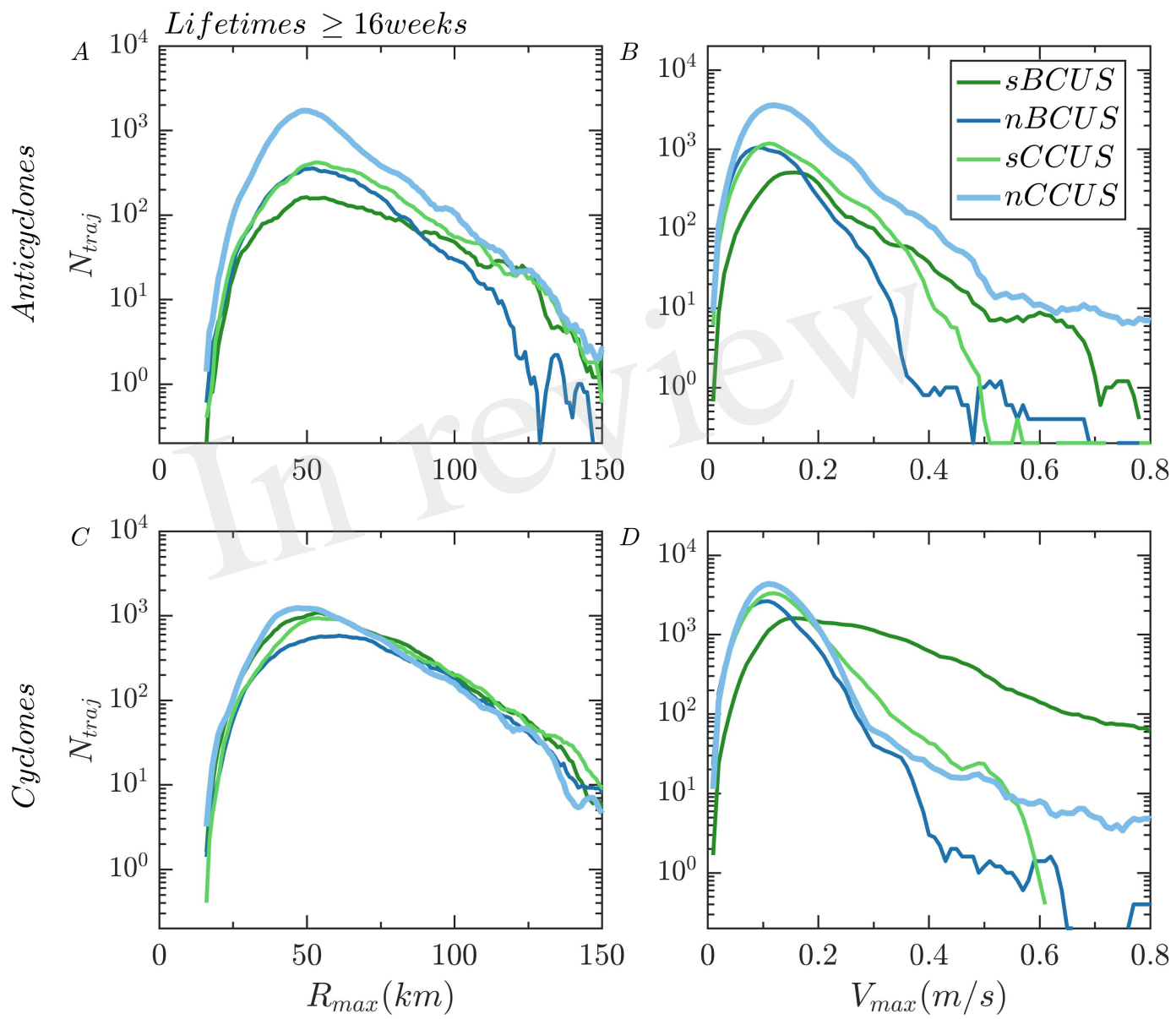


Figure 8.JPEG

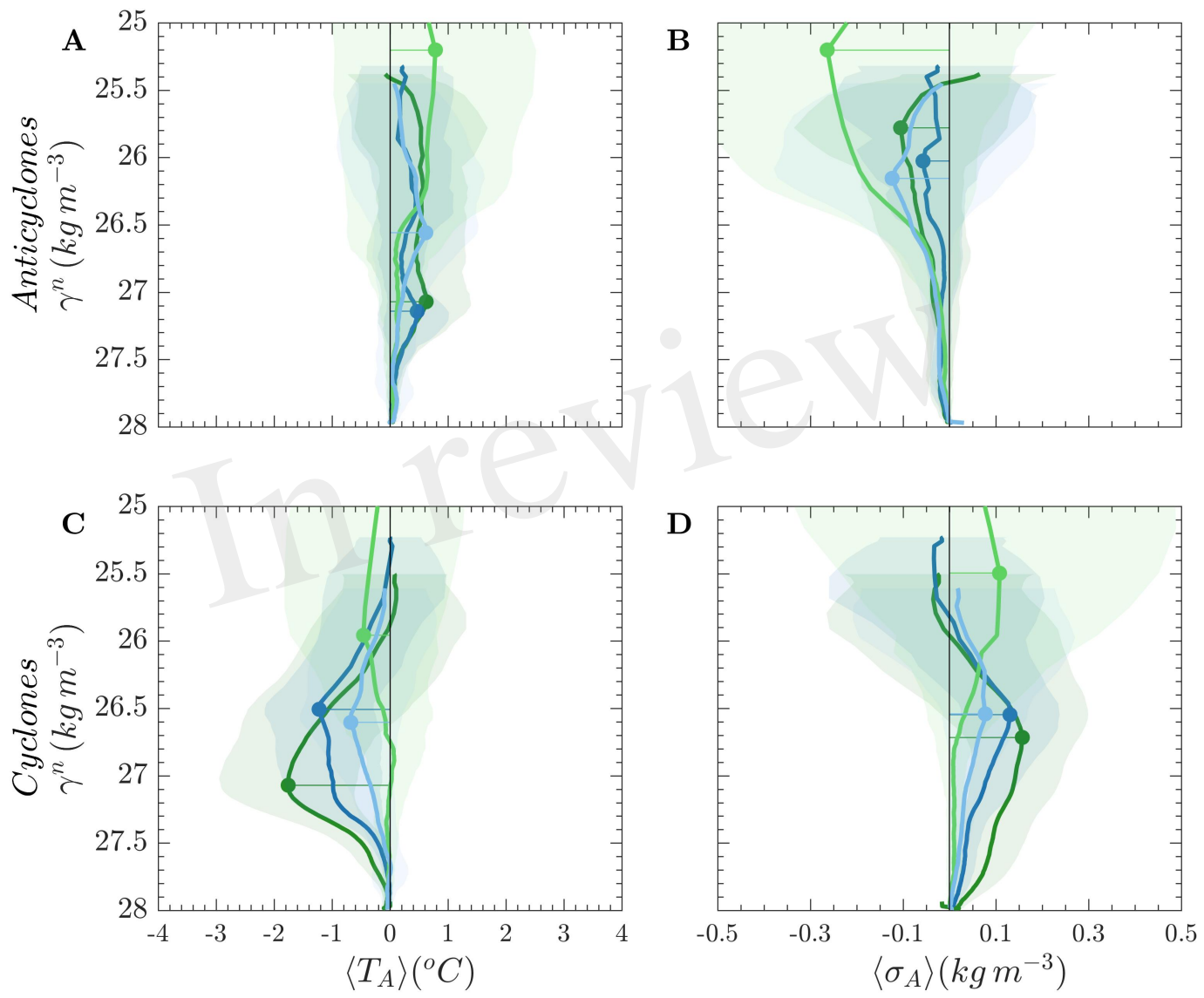


Figure 9.JPG

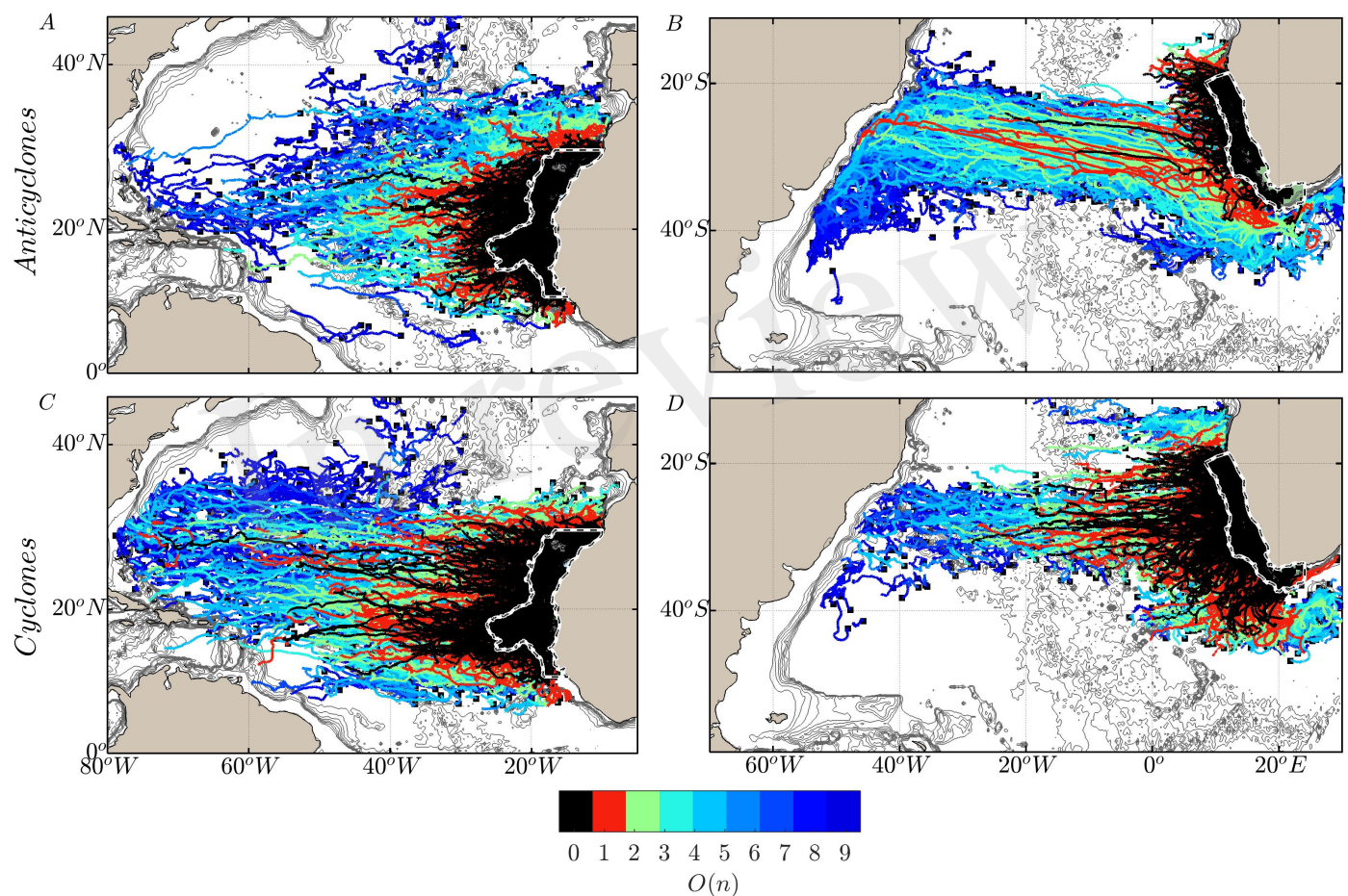


Figure 10.JPEG

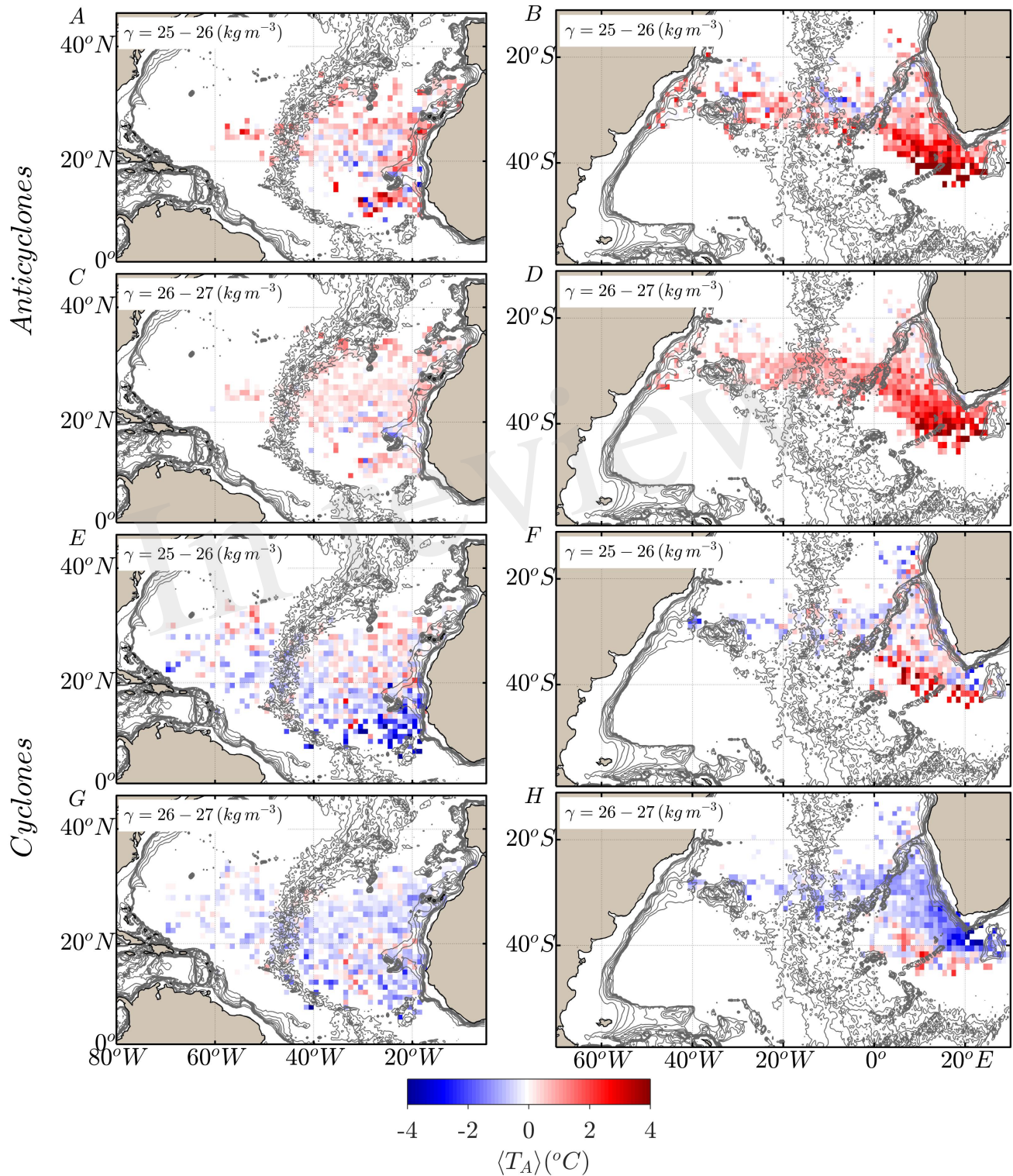


Figure 11.JPEG

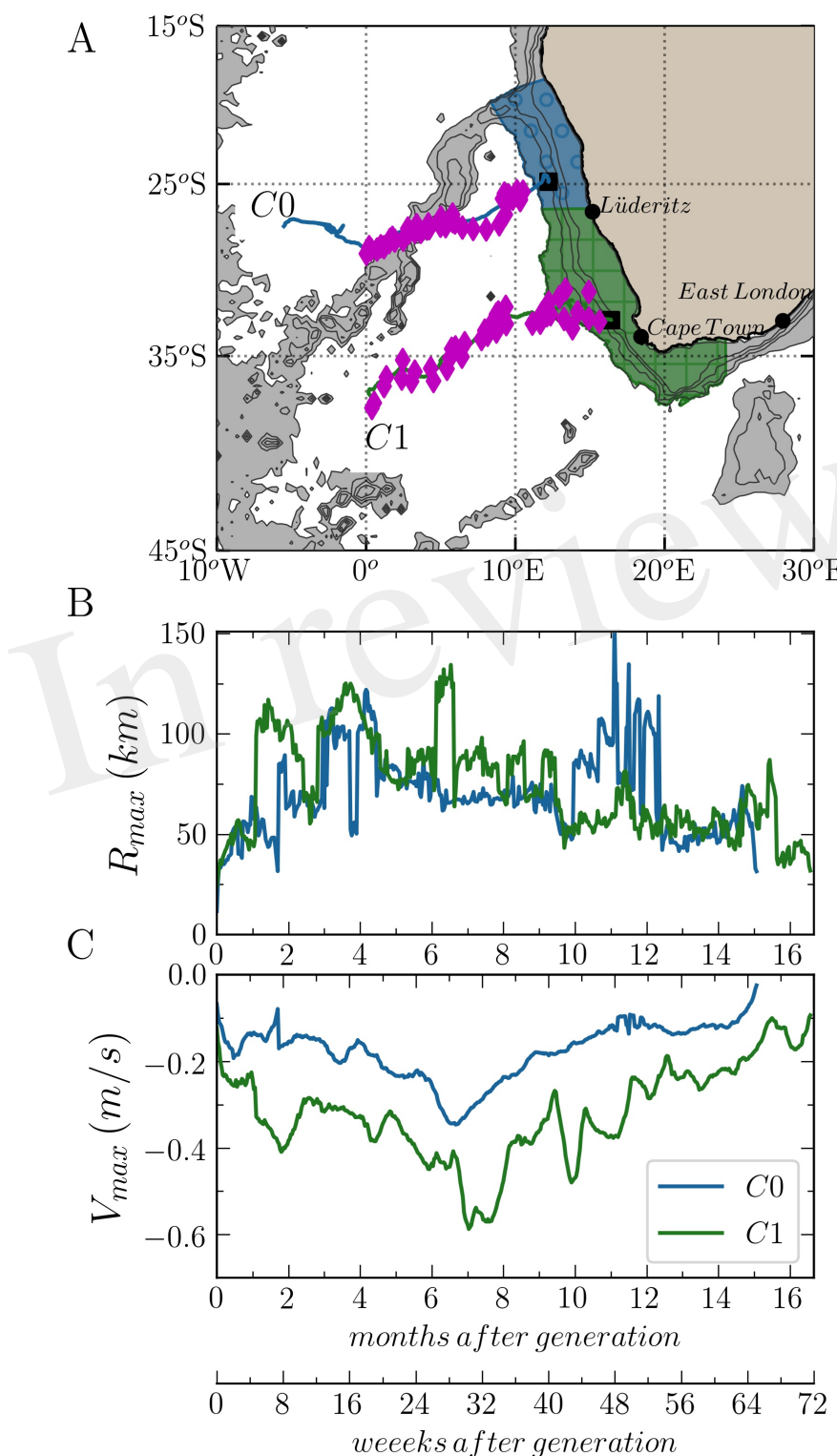


Figure 12.JPEG

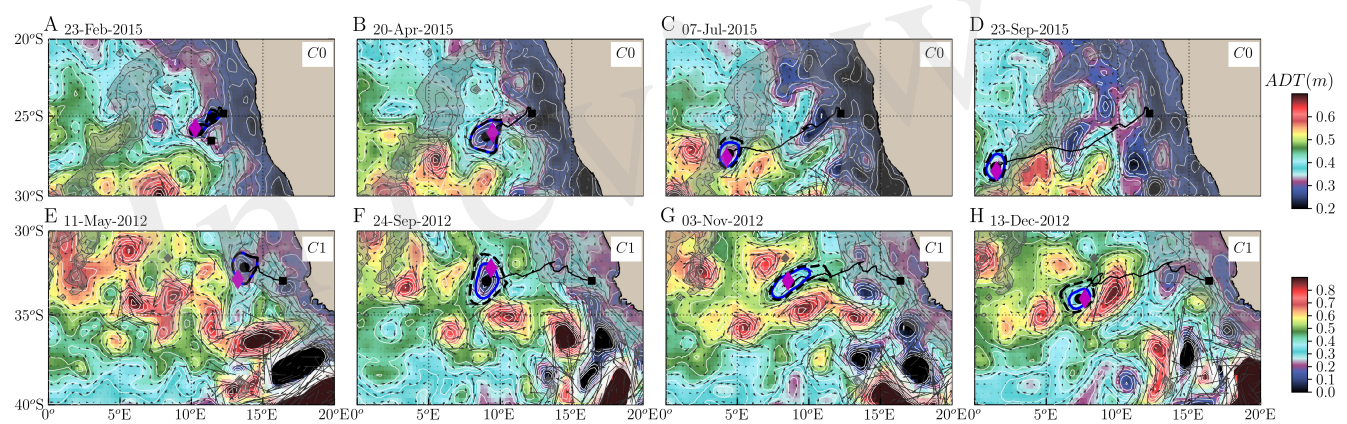


Figure 13.JPG

